Radio Frequency Ablation Lesion Determination Using Impedance Modeling

by

David Akinyele Hampton

Submitted to the Department of Electrical Engineering and Computer Science

in Partial Fulfillment of the Requirements for the Degrees of

Bachelor of Science in Electrical Science and Engineering

and Master of Engineering in Electrical Engineering and Computer Science

at the Massachusetts Institute of Technology

May 27, 1997

Copyright 1997 David A. Hampton. All rights reserved.

The author hereby grants to M.I.T. permission to reproduce and
distribute publicly paper and electronic copies of this thesis
and to grant others the right to do so.

Author_____

Department of Electrical Engineering and Computer Science
May 27, 1997

Certified by_____

Dr. J. Philip Saul, M.D.
Thesis Supervisor

Accepted by_____

Arthur C. Smith
Chairman, Department Committee on Graduate Theses

For my parents,
the two people who have
given me everything

Radio Frequency Ablation Lesion Determination Using Impedance Modeling

by

David A. Hampton

Submitted to the
Department of Electrical Engineering and Computer Science

May 27, 1997

In Partial Fulfillment of the Requirements for the Degrees of
Bachelor of Science in Electrical Science and Engineering
and Master of Engineering in Electrical Engineering and Computer Science

Abstract

Lesion size is the critical parameter in determining radio frequency ablation effectiveness. Inadequate lesion formation can lead to repeated applications and possibly further complications. Investigations into factors influencing radio frequency catheter ablation lesion generation were performed in an effort to create a working model of the catheter-tissue system. Left ventricular free wall tissue was examined through several temperature controlled catheter ablation experiments, and impedance and power correlations to lesion size were made. With the introduction of pulsatile bath flow and continuous sheath flows, lesion volumes were found to increase in depth while remaining fairly constant in width and length. While it was deduced a purely thermodynamic model could not be used in the determination of lesion radii, several critical factors could be exploited in deriving approximations of the actual lesion volumes.

Thesis Supervisor: Dr. J. Philip Saul, M.D.
Title: Harvard Medical School, Department of Pediatrics, Associate Professor
MIT/Harvard Health Science and Technology

Acknowledgments

I would like to thank my thesis advisor Dr. J. Philip Saul for his assistance, patience, and ability to provide light hearted humor which I still have trouble understanding today; Dr. Mark Alexander, Senior Fellow in Cardiology/Electrophysiology at Boston Children's Hospital, for the much needed support, both in research and in my career decisions; Dr. Ronn Tanel, Fellow in Cardiology, for the use of his observations, the staff (Mark, Pascal, and Chrissy) of the Cardiac Surgical Research facilities at Boston's Children's Hospital for their much need help and lively conversations; my academic advisors, Dr. Martha Gray and Professor Mildred Dresselhaus, for never understanding why I do what I do but always finding a way to give me support when needed. I would especially like to acknowledge those people who have been behind me from the beginning: Yuni Sarah Politz, a good friend, who always had more faith in my abilities than I, Yukie Ishitani, for pushing me to try harder, and again to all my family for their undying love and support through the years. Thank you everyone.

Table of Contents

List of Figures

Chapter 1 - Purpose of Research

Radio frequency (RF) ablation has been used to treat many cardiac arrhythmias. Long slender catheters are inserted into the heart via blood vessels. Application of RF energy allows for selective tissue destruction and interruption of tachycardias. The principle mechanism of this techniques is ohmic heating. Ohmic heating is the product of charged particles passing through a resistive material. In our scenario, ionic species within the tissues are attracted to the alternating fields, as they rub and collide against one another they create heat, which in turn creates the lesion. This catheter techniques has an over 95% success rate, in more clinical settings.

One of the biggest challenges in RF ablation is to accurately predict and correlate lesion size. Without this knowledge the technique has been reduced to secondary means of determining the quality of the lesion generation and its effectiveness. The success of the application is usually determined by reviewing directly recorded electrical tracings of the heart's activity. This is a fairly reliable measure when there are clear electrical endpoints. However in infants, where there is a need for small lesions, and in complex atrial and ventricular arrhythmias with a need for large lesions, there is an increasing need to be certain that anatomically directed lesions are actually created. The need to fully understand the ablation process and optimize its parameters is imperative to improving the overall process.

In-vitro experiments have been a useful parallel to the ongoing clinical experience. Their results are reproducible with marginal deviations. These idealized laboratory cases have been able to use the tip temperature as a gauge in lesion control and formation. These lesions have been consistent in morphology and predictability. Conversely, the in-vitro lesions' successes and failures depend upon multiple variables. There are many anatomical and functional variables such as oscillating blood flow, tissue/tip contact, local anatomy, catheter movement from the operator, cardiac contraction and respiration that may affect lesion formation. However, the clinical success and failure is also dependent upon correct mapping and placement of lesions. Because of continued clinical challenges and the controlled nature of in-vivo experiments, laboratory research continues to be a role for in-vitro characterization of this clinically proven technology.

Models incorporating the thermal interaction of the tip and tissue, power delivered, temperature limitations, active tip cooling or mode of ablation, have been developed. Each of these factors have been found to play a significant role in the entire process. The goal of this research was to characterize some of the variables in lesion creation, quantify how they relate to lesion size, and then make a generalized reproducible prediction on the lesion size under various conditions.

Chapter 2 - Physiological Background

In 1979, Vedel et al. [1] performed the first DC catheter ablation producing permanent atrioventricular (AV) block. Unfortunately this technique was plagued with complications such as creating new arrhythmias, cardiac tamponade, and sudden death. These complications were the product of large amounts of energy (100 - 400J) released from the catheter tip. This massive discharge caused localized temperatures to rise approximately 5000^{o}C in a very short time, leading to light, plasma and liquid vapor [2]. The expansion and contraction of this vapor often led to destructive pressure waves within the cardiac chambers. Other complications such as catheter recoil, cardiac perforation and remote tissue injury were also present. Due to these findings, DC ablation use was limited. Other forms of lesion formation had to be investigated.

Energy sources such as microwaves, cryoagents, lasers and radio-frequency energy were investigated. Microwave heating is dependent upon the antennae's construction characteristics, its frequency, and the geometry of the antennae with respect to the tissue. It has advantages of heating tissue not in direct contact with the antennae and the area of heating is somewhat larger than that of the radio frequency (RF) technique used currently [3-6]. Unfortunately catheter design has limited the ability to control lesion placement and size.

Cryoablation, freezing the tissue, has been used successfully to modify and destroy AV conduction in animals [3,7], and is used routinely during open-heart surgical procedures. However, catheter construction and the need for direct application of the cryogenic agent has been a limiting factor. Laser ablation techniques are currently under development. Laser ablation will have the power to produce a large temperature change in a small area and has been used successfully to ablate ventricular tissue in animals and humans [3,8-10]. However this technique has been plagued with the same problems as DC ablations, particularly transmural lesions and myocardial perforation. While these techniques were plagued with application complications, the use of radio frequency energy proved more favorable.

Radio-frequency (RF) catheter ablation (RFCA) has been used to treat many cardiac arrhythmias. Thermal destruction of the cardiac tissue, is primarily due to resistive heating of the cardiac tissue at the electrode/tissue interface [11]. Deeper lesions are generated due to conduction of heat through the tissue and convection within the immediate region of the catheter tip. Lesion formation is dependent on electrode size, temperature at the interface, and the amount of electrode/tissue contact. Catheter ablation is primary used in the treatment of atrioventricular (AV) nodal reentrant tachycardia, AV reciprocating tachycardia, ventricular tachycardia and primary atrial tachycardias. RFCA has over a 95% success rate for eliminating accessory pathway mediated arrhythmias and atrioventricular nodal reentry tachycardia

RFCA uses an unmodulated sine wave at frequencies of 300 - 500KHz. These frequencies are high enough that they will not induce myocardial depolarization within the heart [12]. RF ablation is usually applied in a unipolar fashion between the ablation elec-

trode and a grounding pad on the patient's body. It can also be performed in a bipolar fashion between the proximal and distal electrodes of the ablation catheter, or between two catheters placed on opposing sides of the target tissue.

During the RF energy application, current travels from the electrode to the grounding pad. The intervening tissue is subjected to resistive heating. The heating is proportional to the square of the current density, and current density is inversely proportional to the square of the distance from the electrode

$$J = I/(4\pi r^2)$$

$$h \propto (\rho J)^2$$

$$h \propto \rho \frac{I^2}{16\pi^2 r^4}$$

Heat, h, is proportional to the total amount of current introduced in the tissue. The largest amount of heating and therefore formation will occur near the electrode tip where the surface area is low and the current density is largest [13].

Deeper local lesion formation occurs primarily due to passive heat conduction. At the grounding pad, no significant heating occurs due to the large surface area and current loss between the electrode tip and skin. Precautions are taken, such as the application of conducting gels, to eliminate burning and discomfort from fringing effects along the grounding pad's edges due to locally high current densities can result from the

The efficiency of tissue heating and lesion formation in RF ablation is related to the heat loss, which occurs in two ways - conduction or convection. The circulating blood is a thermodynamic element contacting the surface of the tissue resulting in a non-hemispheri-

cal shaped lesion. Second, the flow through vessels, particularly the epicardial coronary arteries, may withdraw a significant amount of heat. To a much smaller extent, microvascular blood flow may remove heat, though this effect is often neglected, experimental data are inconclusive as to its role.

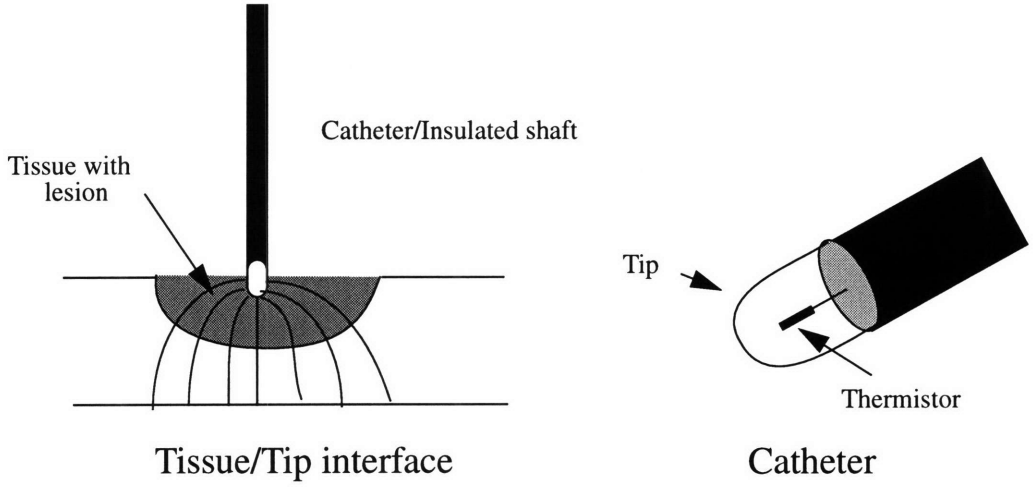

Figure 2-1 Catheter examples - Impaling tissue and catheter tip with thermistor

The observance of the tissue/catheter interface temperature is a method to gauge the lesion size. [1] The depth of tissue heating is a direct result of thermal conduction from the radius of tissue around the electrode (see fig. 2-1). The maximal heating occurs at the smallest area of tissue tip interfacing this results in a higher current density. Below $50^{o}C$ ablation is ineffective. Above $50^{o}C$ lesion formation occurs, however efforts are made to keep the tissue tip temperature below $100^{o}C$. Above this temperature coagulation forms on the catheter tip producing large rises in impedance. [14]

A brief review of the heart, its anatomy and conduction properties, is required before proceeding further. The heart itself is composed of three types of muscle: atrial, ventricular and specialized conduction fibers, in addition to valves and a supporting skeleton of connective tissue. During each heart beat, blood passes sequentially through the right atrium, right ventricle, pulmonary artery, lungs, pulmonary vein, left atrium, left ventricle,

and aorta with flow to the systemic system and returning to the heart via the vena cava (see fig. 2-2). The low pressure, venous side receives deoxygenated blood which is then passed through the pulmonary system and into the left side of the heart. The left heart pumps against the high pressures of the systemic circulation and forces oxygen rich blood into the body. The cardiac output of 3-5 L/min/m^2 is pumped through the system. The action of the heart, is the result of the coordinated contraction of the myocytes.

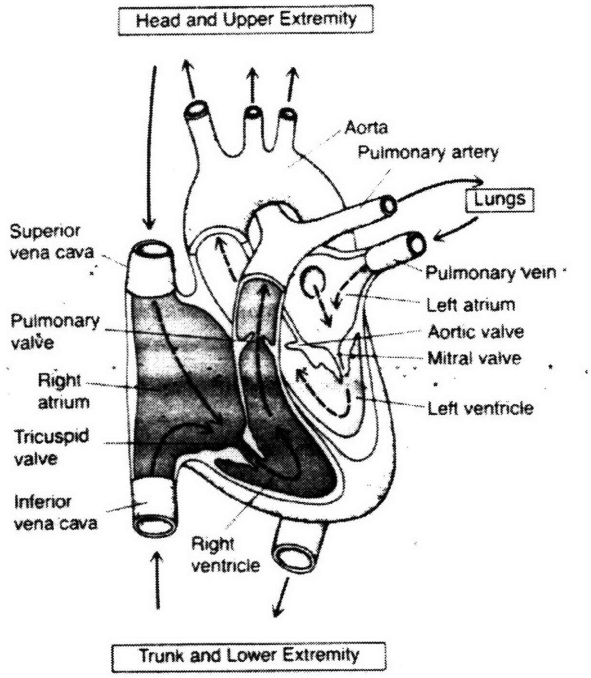

Figure 2-2 - Anatomic structure of the heart [15]

The resting potential for cardiac muscle cells is approximately -85 to -100 mVolts. The cardiac action potential, the depolarization wave which traverses across the heart, has a peak to peak amplitude of 105 mVolts, with a 20 mVolts overshoot. The depolarization phase is 200 milliseconds (msec.) in the atria and 300 msec. in the ventricle. The plateau regions of the potential are 3 to 15 times longer than in skeletal muscle. This is caused by fast sodium channels and slow calcium channels opening nearly simultaneously. The slower channels remain open extending the plateau.

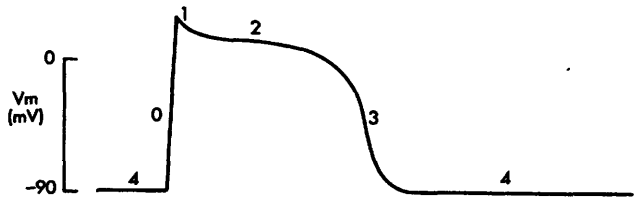

Figure 2-3 - The cardiac action potential

Additionally the potassium permeability decreases about 5-fold, thus lowering the outward flux of potassium and preventing the early recovery in the muscle fibers. When the calcium and potassium channels close, the potassium permeability increases and the membrane's potential returns to its resting state. The flux of ions across cell membranes is regulated by active pumps, concentration gradients and electrochemical gradients. The electrochemical gradients are governed by the Nersnt equation.

$$V_i = \frac{RT}{z_i F} \ln \frac{\eta_i^{inside}}{\eta_i^{outside}}$$

R = gas constant, 8.2 joules/mole degree K

T = the absolute temperature, degree K

F = Faraday's constant, 9.65×10^4 coulomb/mole

Z_i = Valence of the i^{th} ion

η_i = molar concentration of the i^{th} ion

The action potential causes both excitation-contraction coupling to occur and the myofibrils of muscle to contract against one another. The potential travels through the cardiac membrane, into the interior of the cell, and along the membrane of the T tubules. The T-tubules communicate and trigger the release of calcium from the sarcoplasmic reticulum. This catalyzes a reaction between the actin and myosin fibers and contraction occurs. At a

cellular level this occurs over milli-seconds with the aggregate ventricular myocardium depolarization of 40 - 100 msecs. The increase in calcium concentration is directly related to the strength of the cardiac muscle contraction.

The sum of the action potentials can be mapped over time in the surface electrocardiogram (ECG) (see fig. 2-4). The initial portion of the waveform corresponds to the depolarization of the atria, noted as the P wave. The large QRS complex, represents the depolarization of the ventricles. The final wave, the T wave, is the repolarization of the ventricle. Depending on the morphology of these components and the timing between them allows inferences of the cardiac anatomy and physiology. There are other artifacts and features contained in the ECG which are beyond the scope of this report.

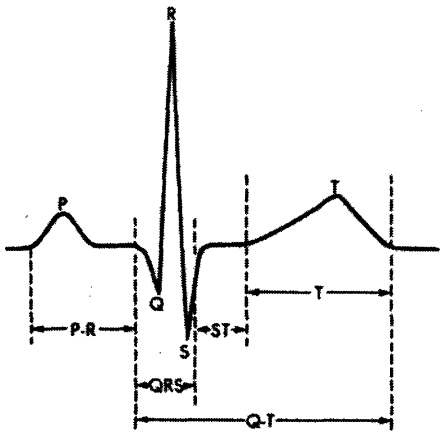

Figure 2-4 An ECG - One cardiac cycle [16]

In a similar fashion uni- and bipolar intracardiac recordings, electrocardiograms, allow for precise spatial localization of the electrical activity.

These electrical depolarizations travel through the local myocardium. They can move rapidly through cell-to-cell connections and gap junctions, or they move slowly, steadily

and irregularly (anisotropically) across cells that are not aligned end-to-end. Associated with this passage is the refractory period which occurs immediately after the excitation of a region of tissue. During this period the normal cardiac pulse cannot re-excite the cardiac muscle. The recovery characteristics of the cell's ion channels determines the absolute and relative refractory periods of the cell. The aggregate of the regional myocyte characteristics determines the clinical refractory period. These characteristics vary by location - the atrial cells are shorter than the AV node's which are shorter than the ventricular cells; age - the cells in younger animals are shorter than in older animals; and the sympathetic state, drugs and metabolic conditions. The normal period for this is 200 - 300 msec. A relative refractory period occurs during which the muscle can be excited with a larger impulse. This refractory period is much shorter in the atria than ventricles so the atrial rate can be much faster.

Returning to the conduction system, within the specialized conduction system the depolarization wave travels between 0.02 to 4 meters/second. There are two locations, sinus node and artio-ventricular (A-V) node, which have an inherent automaticity, the ability to maintain regular and neuro-hormonally regulated depolarizations. The sinus node is the normal origin of the action potentials. These impulses are conducted through the internodal pathways and atrial tissue to the atrio-ventricular node. The impulse is delayed before passing through to the ventricles due to the slowed conduction at the artio-ventricular node. This delay also assists with ventricular filling, hence increasing the stroke volume. Within the ventricle, the left and right bundles of the Purkinje fibers innervate the lower portion of the heart. These are fast conduction pathways allowing for synchronized contraction from the apex of the heart upward.

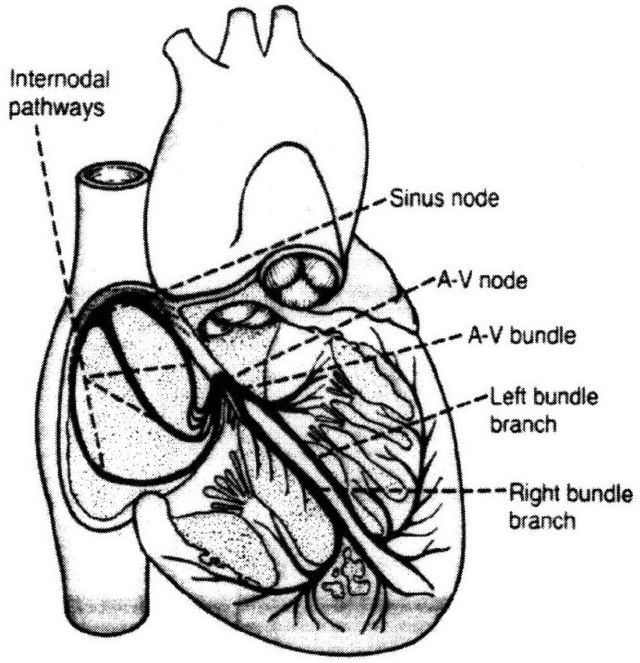

Figure 2-5 - Conduction pathways in the heart

Looking again at the sinus node and its function, it is a small flattened ellipsoid, approximately 3 mm wide, 15 mm long, and 1 mm thick. It is located on the superior lateral wall of the right atrium (see figure 2-5). It contains no contractile filaments. The fibers are continuous with the atrial fibers, therefore any action potential that begins there spreads immediately. Its resting potential is -55 to -60 mVolts due to the membrane being leaky to sodium ions. At -55mVolts the fast sodium channels are essentially inactivated/ blocked. The sodium slowly leaks inward until the membrane potential reaches -40mVolts at which point the calcium and sodium channels open and cause excitation. This depolarization wave travels at 1 m/sec through the anterior, middle and posterior internodal pathways which terminate at the atrio-ventricular (A-V) node.

The A-V node acts as a delay for the propagation. This delay allows for continued emptying of the atria as mentioned before. The A-V node is located on the posterior septal

wall of the right atrium behind the tricuspid valve adjacent to the opening of the coronary sinus. The action potential duration in the A-V node is 130 msec, having been delayed 90 msec, in the node itself and 40 msec. when penetrating the A-V bundle. This decrease in conduction is due to the reduced cross-sectional area of the fibers, a decrease in gap junctions and change in cell orientation. Also the potential does not maintain its original morphology due to a different balance of local ion channels. With an increased resistance and a decrease in voltage the current, the action potential amplitude, is decreased.

From the A-V node the potential enters the Purkinje system. This system allows for the spread of potential through the left and right ventricles over a period of 30 seconds at a velocity of 1.5 to 4.0 m/sec. This rapid transmission is caused by the increased number of gap junctions and their increased permeability. Conduction in this region is usually one-way unless an abnormal event damaging the tissues has occurred. Such abnormal events (e.g. myocardial infarction) may lead to reentry loops, or reexcitation of an area through which the depolarization wave has already passed. This sometimes occurs on a fixed pathway or a random pathway. The random pathway leads to fibrillation. Reentry through an effected region is usually unidirectional. The antegradely conducted pulse may hit refractory tissue and be extinguished or if the delay is long enough it will be conducted toward the origin. For this to occur the effective refractory period of the region must be less than the propagation time around the loop.

Figure 2-6 presents four conditions. Condition A is normal conduction, The depolarization wave traverses normally down both branches, When a transverse pathway C exists, the wavefronts will cancel themselves out. Condition B demonstrates complete blockage of the conducted wave form, the waveform is terminated before it can proceed to the lower

portion of the heart. Condition C nearly demonstrates an example of a reentrant loop. One branchway is open for conduction while the other is abnormally affected and the wave front cannot travel down or up branch R. Trouble begins to occur in D, where the wave front is able to pass through the effected area and return toward the origin. Branch R provides a unidirection pathway for the wave front to circle around, this is the reentry loop. Reentry loops are the most frequent cause for several arrhythmias treated by RF ablation techniques.

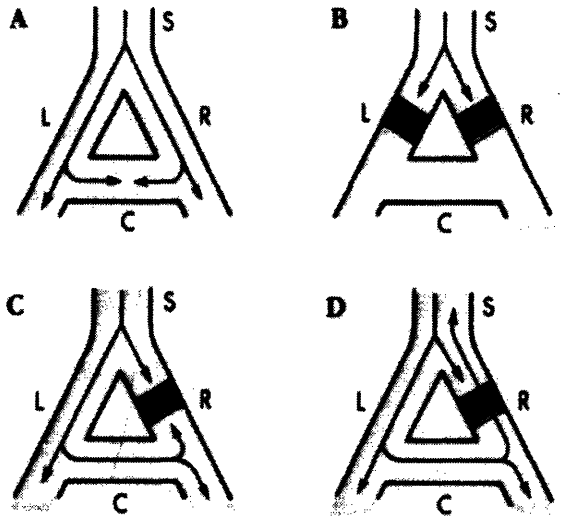

Figure 2-6 Reentrant examples [16]

Figure 2-7 shows the time course of two cardiac cycles. Each cycle consists of four stages: Isovolumic contraction - where the ventricles contract, building up pressure; ejection - where the oxygenated blood is forced into the systemic circulation and deoxygenated blood into the pulmonary system; isovolumic relaxation - where the ventricles relax after displacing their contents and filling - where the blood from the venous system enters the atria begin to fill the ventricles. The heart sounds shown represent the oscillations of blood and closure of valves at different times during the cardiac cycle.

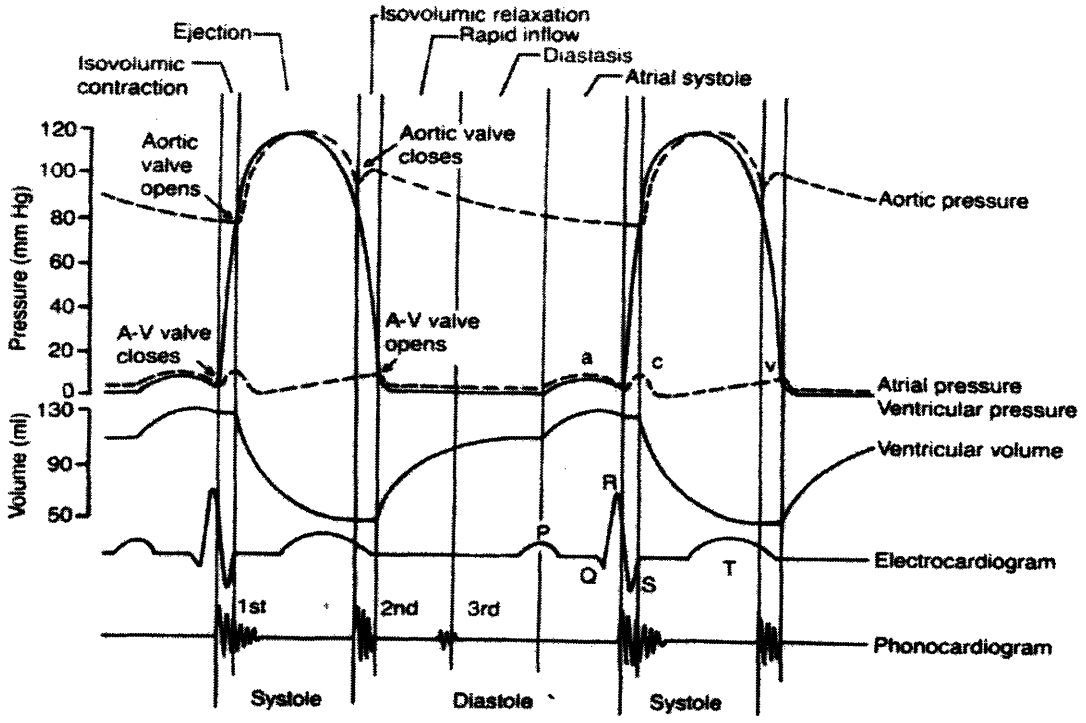

Figure 2-7 The cardiac cycle - Pressure waves measured from the heart [15]

One application of RF ablation is the treatment of WPW, Wolff-Parkinson-White syndrome. This is a typical accessory pathway mediated tachycardia. Accessory pathways are abnormal areas of tissue with conduction characteristics which allow reentry to develop between the atrium and ventricles. They provide an electrical short circuit where an impulse from the atria is often conducted to an abnormal site in the ventricles prematurely. A so-called Bundle of Kent is one example of an accessory pathway. This is a rapidly conducting segment of tissue, other than the AV node, which extends from the atria to the ventricle, bypassing the nonconducting regions of the heart and producing "preexcitation" of the ventricles. It may also conduct retrograde from the ventricles to the atria.

The antegrade pre-excitation allows the potential for AV conduction faster than the 200-230 beats per minute that a normal adult's AV node can support. If these action poten-

tials conduct retrogradely then sufficient delay in the AV node may allow ventricular activity to conduct into the atrium via the accessory pathway and create a circuit for typical supraventricular tachycardia, as in figure 2-6, D. Preexcitation is seen as an early deflection in the QRS complex and is often called a delta wave. The two pathways leading from the AV node, one allowing for this early depolarization of the ventricular tissue, can lead to arrhythmias such as supraventricular tachycardia[16]. This occurs due to the reentry to the cardiac impulse either down the pathway or through normally functioning cardiac tissue.

While conceptually first understood by Dr. Paul Dudley White of the Massachusetts General Hospital, the principles of reentry seen in WPW, a circuit, an area of slow conduction (the AV node) and an area of unidirectional block (the accessory pathway) has been proven to explain many of the common tachycardias. Atrial flutter consisting of macroreentrial circuits that involve the right atrium, atrial fibrillation, multiple smaller left atrial reentry circuits and ventricular tachycardia or fibrillation represent similar physiology in one ventricle, albeit with potentially more dangerous hemodynamic consequences.

Chapter 3 - Engineering Background

The electrical processes in the body can be analyzed using simple passive elements. When ions flow through channels and pores and are separated by the cellular membrane, they create potential gradients, voltages. Leakage and movement of these ions, is called current. By using passive elements, resistors - energy dissipation components, and capacitors - energy storage components, a simple network can be created to represent a complex biological system.

To simplify the model some assumptions must be made about the body's tissues, however these assumptions do not always hold[17]:

Linear - the potential gradient, electric field, is proportional to

$$J = \sigma E = -\sigma \nabla \Phi$$

where J is the current density, σ is the tissue conductivity, E is the electric field and Φ is the potential gradient.

Homogeneous - The body tissues have unique conductivities and permittivities but within the individual tissues or organs these will be assumed to not change.

Isotropic - The tissue properties are independent of orientation

Complex Impedance - The resistive properties are frequency dependent

Upon closer inspection of the tissues, the cellular membrane consists of a Phsopholipid bilayer which acts as a protective boundary for the cell. This layer is permeated by several channels and pores used for ion exchange and other transport processes.

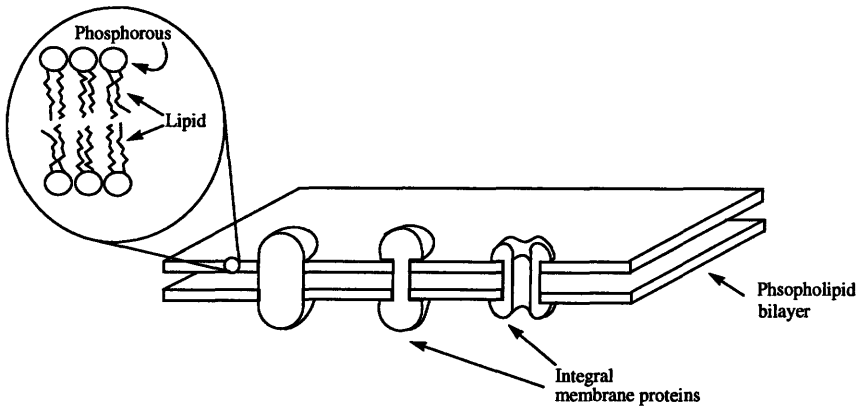

Figure 3-1 - Cell membrane

The lipid bilayer acts like a capacitor. A capacitor consists of two similar layers or plates separating charges. With the charged phosphorous groups extending into the bathing medium and the hydrophobic portion directed inward, these lipids create the plates for the capacitor. The integral proteins, pumps and pores, act like resistors. Each is selective to the various ions and the cell's current state determines the resistance seen to that ion.

Taking the above properties into consideration, a simple model can be developed. The one dimensional cable model is the first approach to understanding the action potential

propagation and how the tissue parameters affect its magnitude. This can also be used to see the affects upon the tissue after changes such as myocardial infarction or radio frequency ablation.

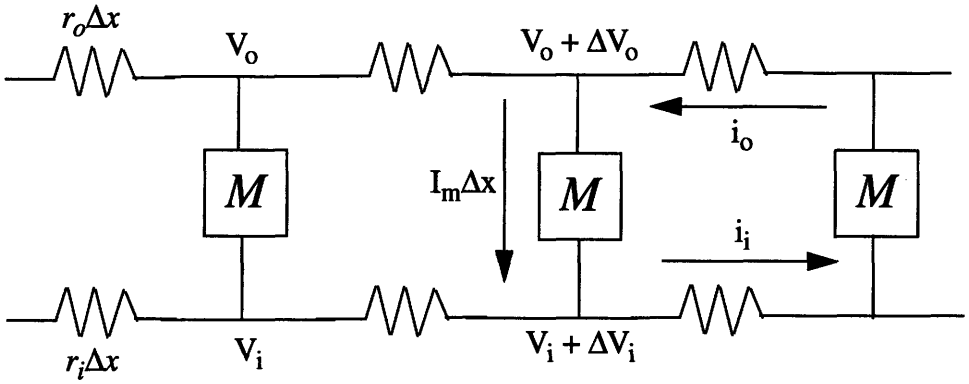

Figure 3-2 - The cable model for a cylindrical cell

The membrane currents flow on the surface of the model and the cardiac cell itself is representative of being an insulative barrier between the inner and outer mediums. The cell interior is represented as a lumped parameter of all the intracelluar elements. This is usually described as a capacitor.

The currents i_i and i_o must be equal and opposite since there are no current sinks or sources. The V_i an V_d are the internal and external voltages. The transmembrane voltage V_m is the difference between the two. This model is derived from Ohms law:

$$i_i r_i \Delta x = -\Delta V_i$$

$$\frac{\partial V_i}{\partial x} = -i_i r_i$$

This equation also holds for the outer conductor. Analyzing the differential voltage across the membrane,

$$\frac{dV_m}{dx} = \frac{\partial}{\partial x}(V_i - V_o) = \frac{\partial V_i}{\partial x} - \frac{\partial V_o}{\partial x} = -i_i(r_i + r_o)$$

$$i_m = \frac{1}{(r_i + r_o)}\frac{\partial V_m}{\partial x}$$

After differentiation and substitution,

$$i_m = \frac{1}{(r_i + r_o)}\frac{\partial^2 V_m}{\partial x^2}$$

This gives us the membrane current per unit length,

$$i_m = C_m\frac{\partial V_m}{\partial t} + \frac{V_m}{r_m}$$

Here C_m is the membrane capacitance per unit length and r_m is the associated resistance. Equating the above two equations for current gives,

$$\frac{\partial^2}{\partial x^2}V_m(x, t) = (r_o + r_i)\left(C_m\frac{\partial V_m}{\partial t} + \frac{V_m}{r_m}\right)$$

This is solved for the time invariant case, the derivative with respect to time equalling zero, we find,

$$V_m(x) = V_o e^{(-x)/\lambda}$$

$$\lambda = \sqrt{\frac{r_m}{r_i + r_o}}$$

The membrane current will have the same function as the voltage. The space constant, λ, is a measure of the distance from the origin to the point where the amplitude of the potential has decreased by a factor of 1/e. Since the model being developed is interested in the change in material properties, the conductivity and permittivity, the cable model is the basis for an initial approach.

Returning to the ablation procedure, one of the largest concerns is the impedance seen between the catheter tip and the grounding patch. Resistance is defined as,

$$R = \frac{\rho L}{A}$$

Where ρ is the resistivity of the medium, L is path length from catheter tip to grounding pad, and A is the cross-sectional area of the tissue/tip interface. From the view of the system, the area, A, is affected by the size of the grounding pad and catheter, the distance, L, is affected by the distance between the pad and the tip, and conductivity, ρ, is influenced by the forced vital capacity in the lungs, the state of the other organs in the body, and the tip-tissue contact.

Impedance incorporate the frequency dependence of the system. The impedance of the capacitor and inductor are respectively:

$$R(s) = \frac{1}{Cs} \qquad R(s) = Ls$$

where C is the capacitance, L is the inductance and s is the frequency $s = \omega = 2\pi f$. Within the frequency domain these frequency dependent parameters can be manipulated as normal steady-state resistances. The complex interplay between these elements and biological properties, is what determines the impedance seen at the catheter tip.

Efficient power delivery is based upon the resistance/impedance seen. Many factors such as coagulum on the tip, patient volume and surface area, the catheter ablation system's own impedance and the geometric relationship between the tip and grounding pad, all affect the ablation results. [18].

Chapter 4 - Materials and Methods

A series of investigations regarding the relationship between impedance and catheter tip contact were conducted. All experiments were performed in the Boston's Children's Hospital Cardiovascular Research labs. Animal usage protocols were approved by the Children's Hospital's Animal Research (ARCH) committee, an AAALAC approved facility. The animal care was performed with the approval of the Children's Hospital Animal Care and Use Committee, was compliant with *The Guide for the Care and Use of Laboratory Animals* published by the National Institute of Health.

Due to the physiology and size similarities between sheep, lamb and human hearts, sheep and lambs were used as experimental subjects. Each lamb was approximately 20 - 22 days old and each weighed 10 - 15 kgs. Each sheep was 3 - 4 months old and weighed 30 - 50 kgs.

Animals were pre-medicated with a 5cc injection of ketamine (Ketalar) and this was immediately followed by 0.2cc of xylazine a more powerful hallucinogen and muscle relaxant. After the animal was sedated with the anesthetics, it was place on an operating table and restrained. Next the animals were euthanized with an intravenous injection of pentobarbital sodium.

A median sternotomy was performed, care was taken not to cut below the diaphragm or into the neck area. Once the xyphoid process was located, a chest splitter was used to divide the sternum, retractors were inserted and the interior was fully exposed. Small scissors were used to cut away the pericardial sac. The heart was grasped in one hand taking care to place the great vessels between the index and middle fingers. A large pair of scissors was used to separate the heart from the body.

The heart was washed in Krebs-Henseleit to remove any clotting blood and to help revitalize the tissue. A 4 by 6 cm section of the left ventricular free wall was harvested. Afterwards it was sutured to a 20 -25 mm thick, 10 centimeter diameter, piece of beef brisket using 2.0 silk suture. The entire specimen was placed in a grounded aluminum bowl and superperfused with blood or Krebs solution at 37°C to 38°C.

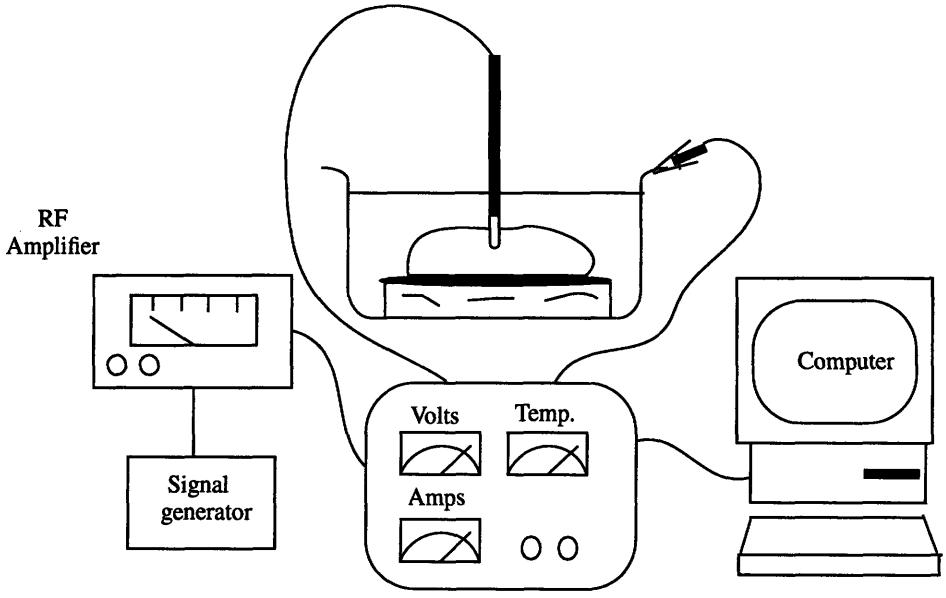

Figure 4-1 Testing apparatus

Three series of experiments were run on the sections of ventricular tissue. The first involved fully penetrating the tissue and sweeping the application voltage from 0.5 to 1

volt. During each application the frequency was also varied from 30KHz to 500KHz. The second trial was kept at a constant voltage but instead varied the depth to which the catheter impaled into the tissue. The penetration depth varied from 0 mm to fully impaled. Two catheter constructions were used. The first was a 10mm cylindrical catheter with an insulated tip, the second was a 5mm uninsulated tip. All test were performed alternately using Krebs and blood as the bathing medium.

A second set of investigations expanded upon the relation between applied power, tip contact and lesion volume using a similar in-vivo model. Beef was substituted for the myocardium. Lesions were generated with a clinical RF generator with the tip/tissue contact standardization using a low frequency (50KHz) impedance measure. All lesions were generated after pressure applied to the catheter produced a 6 - 12 ohm change above the baseline.

This set of tests used a similar testing apparatus; however, a roller pump to vary the bath flow was added to: 1) allow the movement of fluid past the ablation site and 2) to see the affects of cooling the catheter tip. The superfusate bath temperature was held at 37°C while the tip cooling due to sheath flow was maintained at 23-25°C. A standard 7 french (4mm) Marinr catheter (Medtronics, St. Paul, MN) in a 8 French sheath (Cordis) was directed perpendicularly into the tissue. Only the 4mm tip extended past the edge of the catheter. (Figure 4 - 2)

These experiments were run under a temperature controlled regime. The RF Generator was set to apply sufficient power to maintain 70°C as measured by the thermistor embedded in the center of the distal electrode (see fig. 2-1). One series was performed using a

100 Watt, 500 KHz RF generator (RFG3E generator, Radionics, Burlington, MA). A second series using a 50 Watt, clinically available 350 KHz generator (Atakar, Medtronic, Minneapolis, MN)

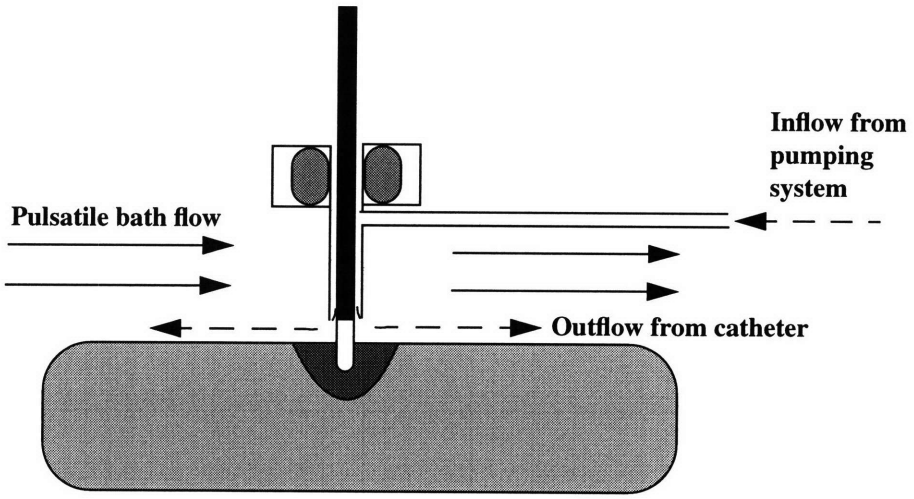

Figure 4-2 Catheter cooling: Flow experimental set-up

Chapter 5 - Results

All data was collected using a Dell 486 (Dell Computer Corp., Austin, TX) and consolidated in Microsoft Excel (Microsoft, Redmond, WA) format and analyzed using Xess (X Engineering Software Systems Corp., Raleigh, NC), a mathematical/statistic package, on a Sun Sparc 4 workstation.

The data taken while superfusing the specimen in blood and kreb is shown separately in Figure 5-1. Both graphs demonstrate an impedance decreased as the frequency is increased. The side by side comparison demonstrates a near identical morphology and numerical values. Also as the applied voltage is increased we see a decrease in impedance. The greater impedance is seen at the lower voltages. The graphs also show a clustering of values at the higher voltages while the 0.5 volt curve appears to be an isolated case.

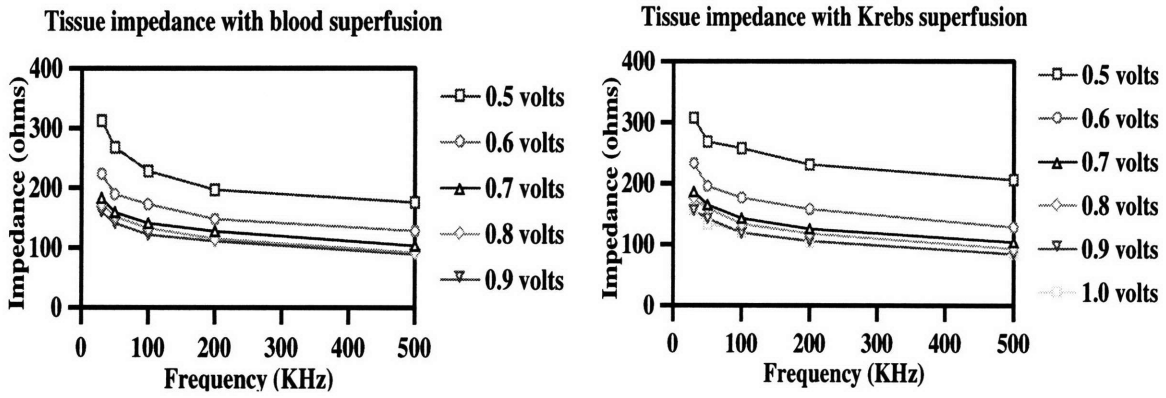

Figure 5-1 Tip/tissue contact - Impedance data from 5mm catheter impaled within left ventricular free wall.

Using a normalized depth (effective tissue penetration divided by catheter length) there was, an increase in impedance as the penetration depth is increased (see figure 5-2). A large increase in impedance can be seen immediately after the catheter touches the tissue. The frequency response seen is similar in form to that of Figure 5-1. Both show a decaying response with an increase in frequency. The greatest impedance is seen at maximum tissue contact and at the lower frequencies. This result matches what was seen in figure 5-1.

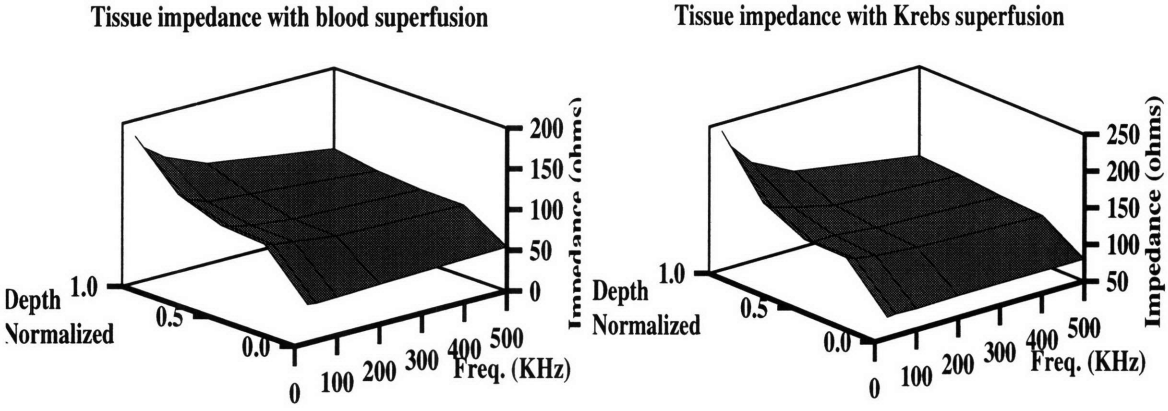

Figure 5-2 Depth vs. impedance - Impedance data given depth and frequency changes. The response varies as both parameters are changed.

A differential comparison, figure 5-3, of the blood and krebs data shows the impedances at each point of interest are indistinguishable. These values were obtained by

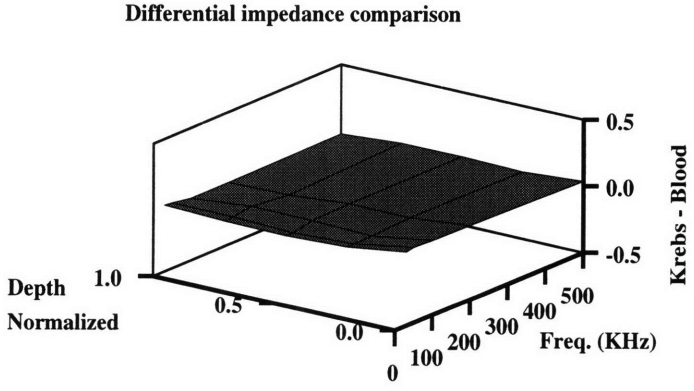

Figure 5-3 Differential comparison

subtracting the impedance seen in the blood by that in the krebs. The largest impedance difference, 0.03 ohms, between the two experimental systems was found at zero penetration depth.

The second set of experiments, the temperature controlled lesion tests, produced results demonstrating the affects of fluid flow and catheter tip cooling on lesions size. The sheath flow was varied from 0 cc/min to 30 cc/min, while the bath flow ranged from 0 L/min to 5 L/min. The actual numerical volume was derived under the assumption of a prolate spheroid geometry where the volume, V is given by:

$$Volume = \frac{2}{3}\pi(depth)\left(\frac{width}{2}\right)^2$$

Bath flow had a marked effect on lesion size. Increases in lesion size were found with increases in bath and sheath flow (see figure 5-4). The increased bath flow appears to produce an offset between the two curves while the increases in sheath flow demonstrate the change in lesion size. The smallest increase occurred at zero flow with an increase of 404% and the largest increase occurred at a 30cc/min sheath flow with an increase of 254%. Two local maximums are found in the zero bath flow curve, one in the low flow regime around 5cc/min and the other at approximately 25cc/min. The 2.5 L/min curve did not show this characteristic.

While the relationship between the width and length of the lesion remained constant with sheath and bath flow, the depth of the lesion mimiced the features of Figure 5-4, therefore the increase in lesion volume seen with both sheath cooling and increases in bath flow is largely explained by the increase in lesion depth. The smallest change, 136%, in

lesion depth resulting from the addition of flow was seen within the high flow regime, while the lower flows presented the greater change, 159%, in lesion size.

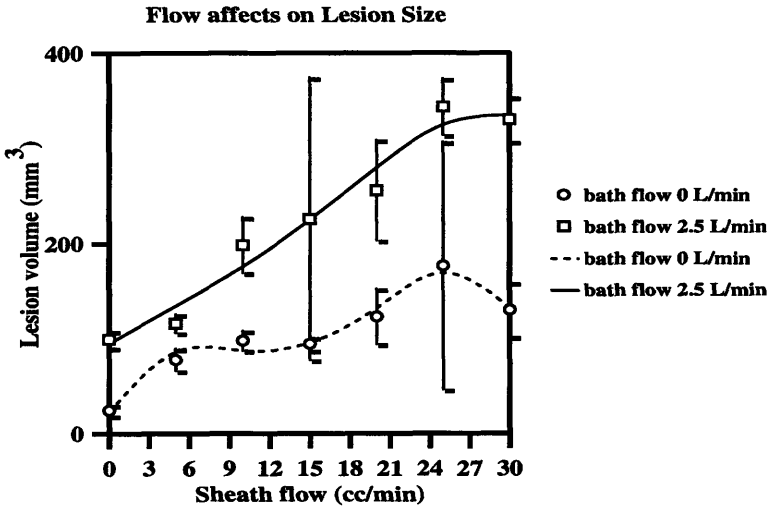

Figure 5-4 Affects of fluid flow on lesion volume - Substantial differences are seen between the volume of a lesion and the flow of the superfusate.

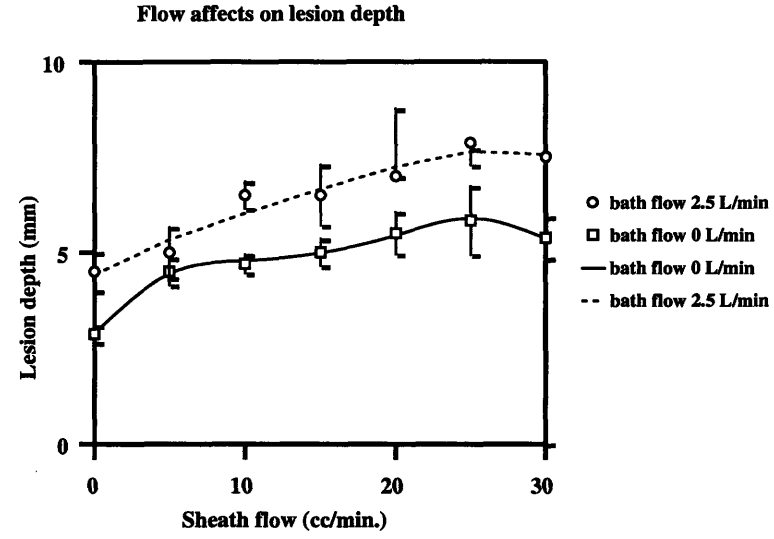

Figure 5 - 5 Affects of fluid flow on lesion depth - The curves mimic the lesion size results.

The power used to create the lesions presented an unexpected response. The larger lesion volumes could only be attained when in the higher flow regimes (see figure 5-6).

The results of the flow tests were nearly identical until the power demand reached 65 watts. At this point the two curves diverged with the higher flow curve continuing to produce the larger lesions.

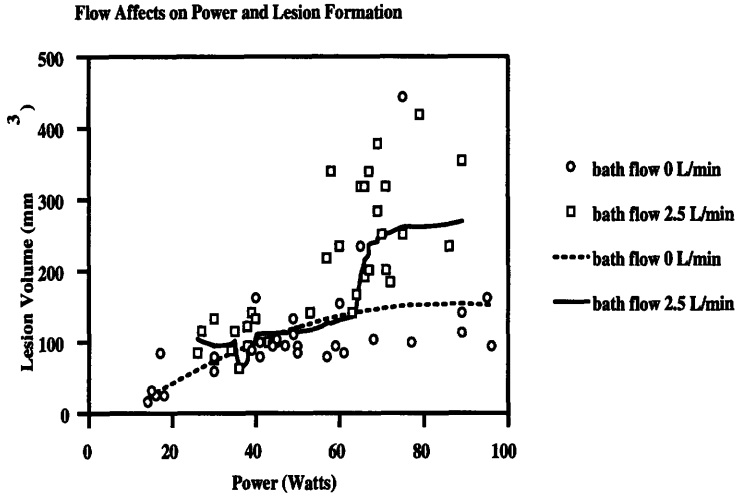

Figure 5 - 6 Affects of fluid flow on lesion formation - Data taken at increasing sheath flows 0-30cc/min from left to right.

The decrease in lesion size directly parallels a decrease in applied power to reach the set temperature. Figure 5-7 shows a decrease in 50KHz impedance leading to an increase in power. The 50KHz impedance was used as a measure to determine the initial placement of the catheter. The initial impedance for the lesion generation tests was a 6 -12 ohms increase above the baseline taken in the perfusate.

These experiments were repeated using a 50 watt generator. In the higher flow states, figure 5-7, a more pronounced maximum is seen and a second local maximum is present. This was not seen in the earlier graphs. Figure 5-7 also shows a characteristic second maximum in all the traces present, the highest result is found in the 1L/min flow curve. As the bath flow continues to increase, the magnitude of the second local maximum decreases.

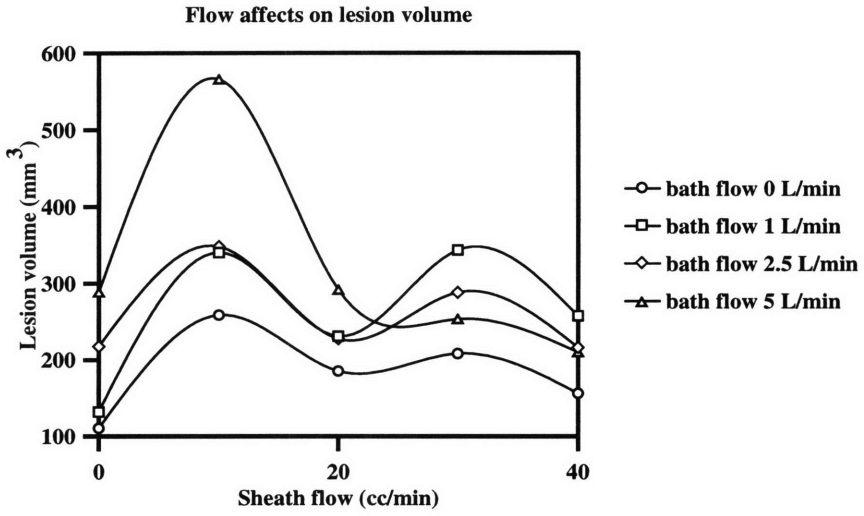

Figure 5-7 Affect on lesion generation at higher flows - These graphs demonstrate a secondary local maximum at higher local flows

A more comprehensive view of the data extrapolates the relationship between bath and sheath flow and lesion volume. The second maximum seen above is isolated in figure 5-8.

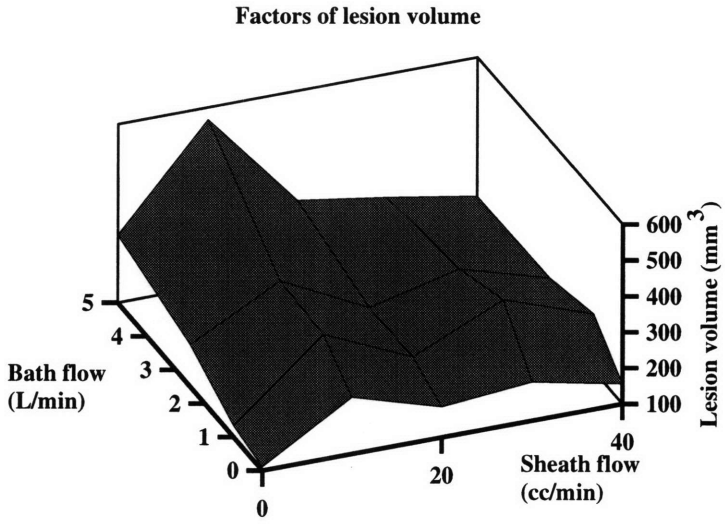

Figure 5 - 8 Extrapolation of fluid affects. The secondary local maximum is a product of both bath and fluid flows.

Changes in bath flow at a constant sheath rate appears to have a greater effect than that changes in the sheath rate at constant bath flows.

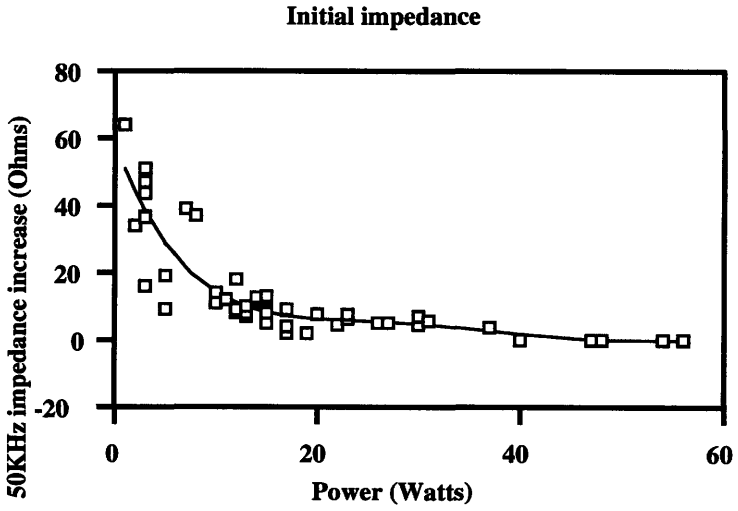

Figure 5-9 Initial Impedance increase

Finally figure 5-9 shows that the closer to the baseline the initial impedance is the greater amount of power the ablation process will use. This is a nearly exponential relation.

Chapter 6 - Discussion

The results obtained demonstrated improved lesion generation when fluid flow was introduced to the system. The incorporation of a variable flow superfusate and sheath flow increased the lesion depth and decreased the total power consumed. The ablation application process also benefited from the non-linear impedance characteristics seen upon tissue-tip contact. The impedance was more sensitive to change at the lower frequencies, 50 - 75 KHz (see fig 5-1). The most notable results in helping to quantify lesion size were:

* Low frequency impedance accurately reflects increased tip/tissue contact, this leads to a better assessment of the effective tip-tissue interface

* Using crabs as a superfusate produces results that are indistinguishable from using heparinized blood, this allows for the interchange of the superfusing medium and to continuing to produce valid data.

* Increasing tip/tissue contact as measured by low frequency impedance produced a bimodal response at the highest recording. Lesion volume decreases with temperature controlled application.

* The decrease in lesion volume parallels a logarithmic decrease in applied power to maintain the set temperature of 70°C.

* While maintaining the same power output, lesion size increased with an increase bath and sheath flow.

The ablation technique centers around the tissue's electrophoretic properties. Electrophoresis is the movement of charged particles in an electrolytic solution induced by an applied E_o field. Every protein and ion has a mobility associated with it. Mobility is defined as the ratio between the applied electric field, E_o, and the electrophoretic particle velocity, U. The motion of the particle is not simply a force balance between qE forces and the viscous friction. qE forces are those seen on charged particles in free space when an electric field is applied. The actual coupling occurs in the mobile part of the double layer where the viscous and electrical shear stresses balance.

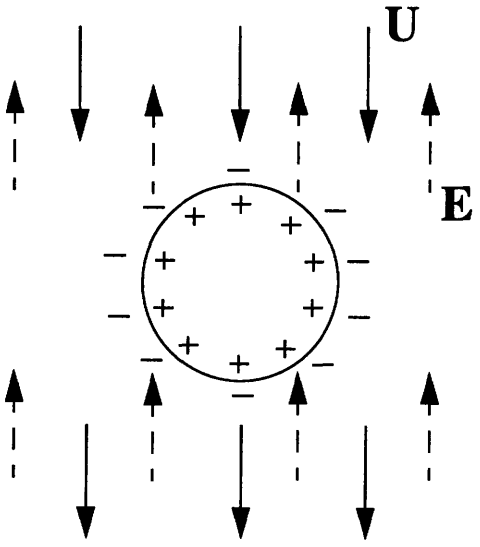

Figure 6-1 Charged particle in an electric field

Before continuing, a brief discussion of the double layer just mentioned is necessary. The double layer can be described as the interface between two phases: 1) the electrolyte which the specimen is immersed and 2) the surface of the specimen itself [19]. If we assume a uniform charge density on the particle's surface and a one dimensional distribution, the following is valid. The potential and charge distribution in space can be given by Poisson's equation:

$$\nabla^2\Phi = -\frac{\rho_u}{\varepsilon}$$

In one dimension this reduces to:

$$\frac{d^2\Phi}{dx^2} = -\frac{\rho_u}{\varepsilon} = -\frac{1}{\varepsilon}\sum z_i F c_{io}(x)$$

Here the charge densities are expressed in terms of the concentrations. The one dimensional double layer can be visualized as:

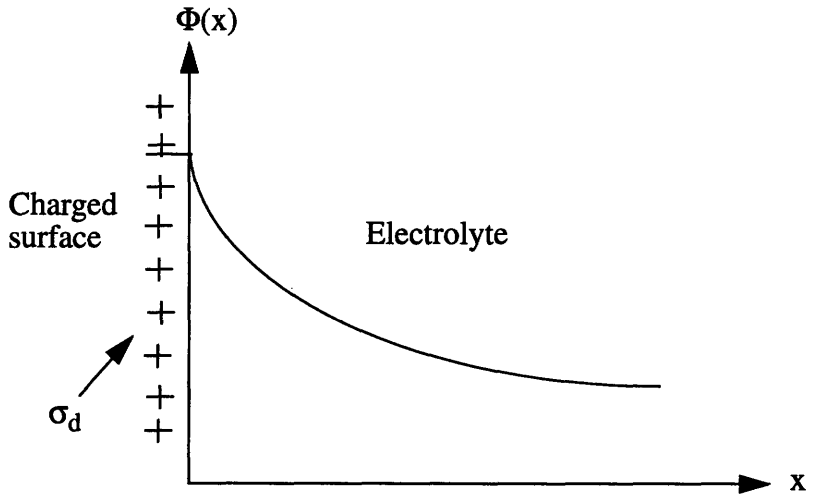

Figure 6-2 - Electric charge distribution

If we assume a Boltzman distribution where we account for the drift and diffusion near the surface, this becomes

$$\frac{d^2\Phi}{dx^2} = -\frac{\rho_u}{\varepsilon} = -\frac{1}{\varepsilon}\sum z_i F c_{io} e^{\frac{z_i F\Phi(x)}{RT}}$$

Solving for $\Phi(x)$, the potential distribution

$$\kappa^2\Phi(x) = \frac{2zFc_{io}}{\varepsilon}\sinh\frac{zF\Phi(x)}{RT}$$

where,

$$\frac{1}{\kappa} = \sqrt{\frac{\varepsilon RT}{2z^2F^2c_{io}}} \equiv Debyelength$$

The debye length is the distance over which the potential drops by 1/e th from its original value. Finding a relation between the surface charge, σ_d, and the surface potential $\Phi(0)$, will give the potential drop across the diffuse layer.

$$\sigma_d = -\varepsilon\frac{\partial\Phi}{\partial x}\bigg|_{x=0}$$

After substitution,

$$\sigma_d = \sqrt{8\varepsilon RTc_{io}}\sinh\frac{zF\Phi(0)}{RT}$$

For $zF\Phi(0) << RT$ (very close to the surface),

$$\sigma_d = \frac{\varepsilon}{1/\kappa}\Phi(0) = \varepsilon\sqrt{\frac{2z^2F^2c_{io}}{\varepsilon RT}}\Phi(0)$$

The above describes a parallel plate capacitor model for the double layer with plate spacing equal to the debye length.

Looking at the electromechanical experiments, it is not the potential drop which is important but rather the fluid's mechanical slip plane. This occurs about 2-3 molecular diameters from the interface and represents the beginning of the mobile portion of the dif-

fuse layer. Over this mobile region the electrical and viscous shear forces equilibrate. The potential across this region is important and is often called the ζ (zeta) potential. This again can be modeled as a simple capacitor:

$$\varsigma = \int_{x}^{slipplane} \frac{d}{dx}\Phi(x)\ dx$$

$$\sigma_{ek} = \int_{slipplane}^{\infty} -\rho_u(x)dx = \int_{slipplane}^{\infty} \varepsilon\frac{d^2}{dx^2}\Phi(x)dx$$

σ_{ek} is equal and opposite to the net charge in the mobile region.

$$\sigma_{ek} = C_{ek}\varsigma$$

Even though several approximations have been made with regard to the system the overall accuracy of slip plane is fairly reasonable. With this overview of the double layer, one of the direct areas of interest, the discussion of ablation will be more clear.

Ablation is concerned with the ohmic heating due to the oscillating electric field applied to the medium. The electrophoretic properties as discussed above play a direct role. The electric fields move charged particles against one another, creating heat and finally the desired lesion. To illustrate this further, we can resolve the mechanics of the problem into a one-dimensional approach which will be elaborated upon; the problem is now a particle in a conducting medium within an applied uniform field. Using a one-dimensional approach, the electric field can be defined as:

$$E = i_x E_o = E_o(i_r\cos\theta - i_\theta\sin\theta)$$
$$U = -i_x U = -U(i_r\cos\theta - i_\theta\sin\theta)$$

The conservation of charge equation requires that the normal conduction current in the liquid phase be balanced by the divergence of the convective surface currents at the interface.

$$n \cdot (J_1 - J_2) + \nabla_\Sigma K = 0$$

Assuming that the double layer is much smaller that the particle's radius, d<< R, we can say:

$$\rho_u(r) \cong -\sigma_m u_o [r - (R + d)]$$

$$\sigma_m = \left(\frac{\varepsilon}{d}\right)\zeta$$

$-\sigma_m$ is the ionic charge in the double layer. The surface charge K can be write as

$$K = \int_R^\infty \rho_u(r) v_\theta(r, \theta) dr \qquad K \cong -\sigma_m v_\theta{}^d$$

Using the conservation of charge equations:

$$-\sigma \frac{\partial \Phi^d}{\partial r} + \frac{1}{r \sin\theta} \frac{\partial}{\partial \theta}(-\sigma_m v_\theta{}^d \sin\theta) = 0$$

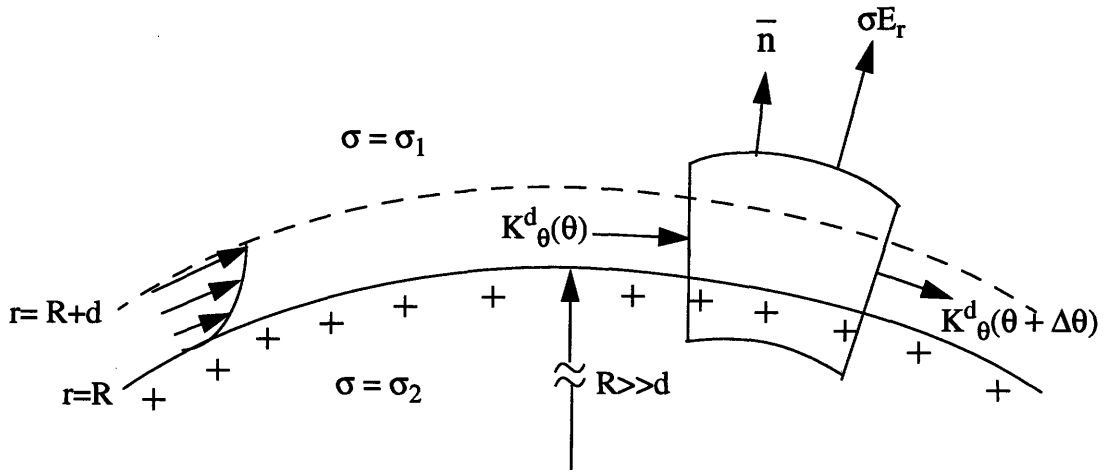

Figure 6-3 Slip plane

Looking at the particle directly, the velocity at the edge of the double layer (see figure 6-3) is

$$v_\theta = v_\theta^{\,d}\sin\theta \qquad v_r = v_\theta^{\,d}2\cos\theta \equiv 0$$

Through direct substitution we have

$$\frac{\partial\Phi^d}{\partial r} = \frac{2\sigma_m v_\theta^{\,d}}{\sigma R}\cos\theta$$

Since there is no charge in the bulk fluid, Laplace's equation can be used. Using Laplace produces

$$\Phi = \frac{A\cos\theta}{r^2} - E_o r\cos\theta$$

From the above boundary condition we can solve for A

$$A = \frac{R^3}{2}\left(-E_o - \frac{2\sigma_m}{\sigma R}v_\theta^{\,d}\right)$$

When d<<R, every section of the surface looks like a flat plane, therefore the problem reduces to that of electroosmosis

$$v_\theta^{\,d} \cong \frac{\varepsilon\zeta}{\eta}E_\theta^{\,d}$$

Using the applied E-field that is tangential to the surface produces

$$v_\theta^{\,d} = \frac{\frac{3}{2}\frac{\varepsilon\zeta}{\eta}E_o}{1+\frac{\varepsilon\zeta\sigma_m}{\eta\sigma R}}$$

The particle is in a force equilibrium, therefore the net force due to the applied electric field and those due to the viscous stresses must be zero

$$f_z = \pi R\eta(-6U + 4v_\theta^{\,d}) = 0$$

Through simple algebra the velocity at the slip plane is found to be proportional to the electrophoretic velocity, U.

$$U = \frac{2}{3} v_\theta{}^d$$

Finally from the relation between the velocity, U, and the applied field, E_0, we obtain.

$$U = \left[\frac{\frac{\varepsilon\zeta}{\eta}}{1 + \frac{\varepsilon\zeta\sigma_m}{\eta\sigma R}} \right] E_o$$

The above electrophoretic velocity alternates between two maxima due to the nature of the applied field E_0, where $E_0 = E\sin\omega t$. With multiple particles in the system each having a specific velocity, the number of collisions increases. Each collision reduces the energy level of the particles, giving off heat. this heating leads to hydrolysis of the cell membrane and finally cellular death and lesion formation.

In deriving a mathematical model based upon the lesion generation data collected, the following flow diagram can be considered:

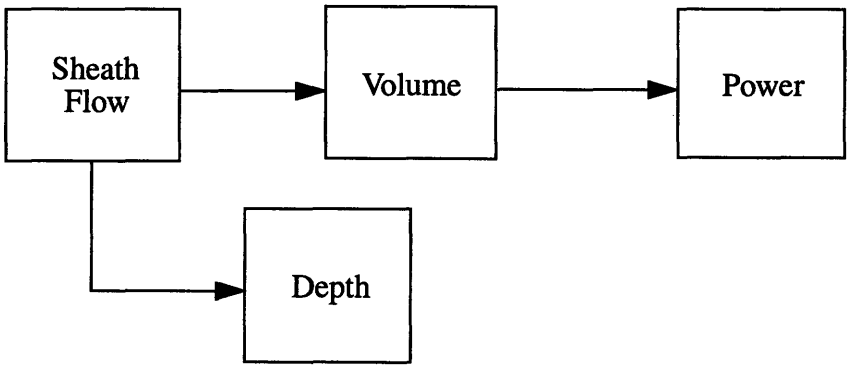

Figure 6-4 Flow chart for mathematical model

The model's predictions are based upon the data for the clinical 50 watt RFCA system, these results hold for the temperature controlled, 70°C case. By considering a pre-deter-

mined sheath flow, the volume and lesion depth can be predicted fairly accurately, ρ = 0.988 and 0.988 for the 0 L/min and 2.5 L/min volume data and ρ = 0.988 and 0.973 for the 0 L/min and 2.5 L/min. depth data.

Stepping through the flow chart above, for the 0 L/min bath flow case:

$$Volume = (-3.218x10^{-3})f^4 + 0.1889f^3 + (-3.514)f^2 + 25.92f^1 + 22.53$$

$$Depth = (-4.4747x10^{-4})f^4 + 2.766x10^{-3}f^3 + (-0.0578)f^2 + 0.5355f^1 + 2.889$$

and for the 2.5 L/min bath flow case,

$$Volume = (-7.129x10^{-4})f^4 + 0.0306f^3 + (-0.302)f^2 + 8.769f^1 + 94.621$$

$$Depth = (-9.848x10^{-4})f^4 + 5.0757x10^{-3}f^3 + (-0.01028)f^2 + 0.2223f^1 + 4.42072$$

In both of the above cases, f is the sheath flow.

After the volume has been determined, the total amount of power required can be calculated, For the 0 L/min bath flow case

$$Power = -9.10045\times10^{-4}V^2 + 0.5482V + 6.69$$

For the 2.5 L/min bath flow case

$$Power = -6.647\times10^{-4}V^2 + 6.44V - 0.499$$

In both cases, V is the lesion volume

Reexamining the equations, the higher order terms, f^4, f^3, and f^2 can be considered negligible due to the small numerical coefficients. Similarly the V^2 terms can be neglected. This reduces the equations to a linear approximation which should give a rough estimate of clinical ablation size when using an initial 50 KHz impedance increase of 6-12 ohms as the baseline measure of contact

For superfusate volumes between 0 and 2.5 L/min, the plane of values between the two curves is fairly linear and an extrapolation between V_0, $V_{2.5}$ and D_0, $D_{2.5}$ and P_0,$P_{2.5}$, where V, D, P represent volume, depth, and power respectively, and the subscripts, the flow rate, can be done. For flows above 2.5 L/min, further testing must be done to fully understand the nature of the high flow curves.

Chapter 7 - Future Considerations

Though one approach has been investigated, this is not the only method of analysis. By using a thermodynamic modeling package, such as IDEAS, Integrated Design Engineering Analysis Software, (Structural Dynamics Research Corp., Milford, OH), a more comprehensive model can be developed and exploited. This model could not only target the lesion area as done for this analysis, but also more accurately represent the thorax region and possibly, given enough time, the entire human. The step from just modeling the tip/tissue interface to the incorporation of influences from the entire body allows all of the internal and possibly external factors to be accounted.

The lesion generation analysis could benefit from a sheath flow medium different than Krebs. Once the exact nature of the sheath flow is defined it could be refined to give deeper lesions. Also the tip geometry could be altered to enhance the lesion process. Whether a blunt or insulated tip catheter is selected or modified, geometric considerations given to the electric field distribution could greatly enhance RFCA, providing a more concentrated or dispersive pattern, producing a variety of lesions.

Appendix

Lesion Volume and Depth Data

Bath flow	Sheath flow	5 Sec. Power	Length	Width	Depth
0	0	14	4	3.5	2.5
0	0	16	4	4	3
0	0	18	4	4	3
0	0	15	4.5	4.5	3
0	5	39	6	6.5	4
0	5	17	5.5	6	4.5
0	5	30	5	5.5	5
0	5	30	5	5	4.5
0	10	41	6	6.5	4.5
0	10	41	5.5	5.5	5
0	10	44	6	6.5	4.5
0	10	45	5	6.5	4.5
0	10	49	6	6.5	5
0	15	50	5.5	6	5
0	15	45	5.5	6	5.5
0	15	50	6	6	4.5
0	15	44	6	6	5
0	20	40	6	7.5	5.5
0	20	61	5.5	6	4.5
0	20	49	6	6.5	6
0	20	47	5	5.5	6
0	20	89	6	7	5.5
0	25	75	10	11	7
0	25	96	5	6	5
0	25	57	5	5.5	5
0	25	59	5	6	5
0	25	65	7	8	7
0	25	89	4.5	6	6
0	30	77	6	6.5	4.5
0	30	95	7.5	7.5	5.5
0	30	60	7.5	7	6
0	30	68	5.5	6	5.5
2.5	0	36	6	5.5	4
2.5	0	27	7	7	4.5
2.5	0	35	7	7	4.5
2.5	0	30	6	6	4
2.5	0	39	8	7	5.5
2.5	0	26	6	6	4.5
2.5	5	40	7	7.5	4.5
2.5	5	53	6.5	7	5.5
2.5	5	43	7	6.5	4.5

Volume		Bath	Sheath	Power	Depth	Volume
16.035199		0	0	15.75	2.875	24.527309
25.13272		0	5	29	4.5	77.852527
25.13272		0	10	44	4.7	97.690359
31.808599		0	15	47.25	5	94.2477
88.488118		0	20	57.2	5.5	123.13724
84.82293		0	25	73.5	5.8333333	176.47445
79.194248		0	30	75	5.375	129.78694
58.904812						
99.549133		2.5	0	32.166667	4.5	99.265517
79.194248		2.5	5	39.428571	5	115.76198
99.549133		2.5	10	65.25	6.5	198.46013
99.549133		2.5	15	73.5	6.5	225.91632
110.61015		2.5	20	68.8	7	256.09194
94.2477		2.5	25	64.75	7.875	343.67686
103.67247		2.5	30	75.333333	7.5	330.1942
84.82293						
94.2477						
161.98823					percentage changes	
84.82293					at no sheath flow	
132.73218						
95.033097						
141.10975						
443.48779					Depth std.	depth high
94.2477					0.21650635	3.0915064
79.194248					0.35355339	4.8535534
94.2477					0.24494897	4.944949
234.57205					0.35355339	5.3535534
113.09724					0.54772256	6.0477226
99.549133					0.89752747	6.7308608
161.98823					0.54486237	5.9198624
153.93791						
103.67247					0.5	5
63.355398					0.65465367	5.6546537
115.45343					0.35355339	6.8535534
115.45343					0.79056942	7.2905694
75.39816					0.89442719	8.7694272
141.10975					0.21650635	7.7165064
84.82293					0	0
132.53583						
141.10975						
99.549133						

Vol. Std.	Vol. high	Vol. Low		line volume
5.6095044	30.136814	18.917805		22.53841
11.429331	89.281858	66.423196		85.92893
10.192077	107.88244	87.498282		87.141834
6.6643188	100.91202	87.583381		95.455759
28.921628	152.05887	94.21561		131.87368
130.17555	306.65	46.298907		169.12289
28.357024	158.14396	101.42991		131.65503
8.8139238	108.07944	90.451594		94.621501
9.7268938	125.48888	106.03509		134.27913
29.17083	227.63096	169.2893		175.53462
148.40129	374.31761	77.515028		225.32717
52.684482	308.77643	203.40746		279.90117
29.508559	373.18541	314.1683		324.80622
23.398661	353.59286	306.79554		334.89713
4.0471425				
404				
depth low				
2.6584936				
4.1464466				
4.455051				
4.6464466				
4.9522774				
4.9358059				
4.8301376				
4				
4.3453463				
6.1464466				
5.7094306				
6.9805728				
7.2834936				
0				

line depth		Power	Volume	linefits
2.8897006		14	16.035199	21.569794
4.4395743		15	31.808599	25.210047
4.7816198		16	25.13272	28.799557
4.9837662		17	84.82293	32.338321
5.4427309		18	25.13272	35.826341
5.8840188		30	79.194248	73.724499
5.3619228		30	58.904812	73.724499
		39	88.488118	97.352753
4.4207251		40	161.98823	99.724391
5.3327922		41	79.194248	102.04529
6.0251623		41	99.549133	102.04529
6.6569264		44	99.549133	108.7035
7.2394481		44	94.2477	108.7035
7.6363636		45	103.67247	110.82141
7.5635823		45	99.549133	110.82141
		47	95.033097	114.90501
		49	110.61015	118.78563
		49	132.73218	118.78563
		50	84.82293	120.64982
		50	94.2477	120.64982
		57	79.194248	132.27832
		59	94.2477	135.14405
		60	153.93791	136.50079
		61	84.82293	137.8068
		65	234.57205	142.52336
		68	103.67247	145.52796
		75	443.48779	150.76264
		77	99.549133	151.80156
		89	113.09724	153.77253
		89	141.10975	153.77253
		95	161.98823	152.01781
		96	94.2477	151.54775
		26	84.82293	104.56268
		27	115.45343	100.93274
		30	132.73218	95.113061
		30	75.39816	95.113061
		34	88.488118	97.359785
		35	115.45343	99.401637
		36	63.355398	69.088743
		38	94.2477	73.926148
		38	121.67116	88.334053

2.5	5	38	5.5	6.5	5.5
2.5	5	34	5.5	6.5	4
2.5	5	30	6.5	6.5	6
2.5	5	38	6	6	5
2.5	10	64	6.5	7	6.5
2.5	10	66	7	7.5	6.5
2.5	10	71	8.5	8	6
2.5	10	60	8	8	7
2.5	15	72	8.5	8	5.5
2.5	15	67	8	8	6
2.5	15	86	8	8	7
2.5	15	69	8	8.5	7.5
2.5	20	70	8	8	7.5
2.5	20	79	8.5	10	8
2.5	20	75	7	8	7.5
2.5	20	63	6	7	5.5
2.5	20	57	6.5	8	6.5
2.5	25	69	9	9.5	8
2.5	25	65	9	9	7.5
2.5	25	67	8.5	9	8
2.5	25	58	8	9	8
2.5	30	71	8.5	9	7.5
2.5	30	89	9	9.5	7.5
2.5	30	66	8.5	9	7.5

121.67116						
88.488118						
132.73218						
94.2477						
166.76607						
191.44064						
201.06176						
234.57205						
184.30661						
201.06176						
234.57205						
283.72485						
251.3272						
418.87867						
251.3272						
141.10975						
217.81691						
378.038						
318.08599						
339.29172						
339.29172						
318.08599						
354.41062						
318.08599						

		39	141.10975	88.334053
		40	132.53583	107.3012
		43	99.549133	111.99953
		53	141.10975	116.68047
		57	217.81691	125.99019
		58	339.29172	125.99019
		60	234.57205	130.61897
		63	141.10975	135.23037
		64	166.76607	148.96026
		65	318.08599	193.59651
		66	191.44064	210.96423
		66	318.08599	215.2627
		67	201.06176	223.80748
		67	339.29172	236.49426
		69	378.038	240.68842
		69	283.72485	244.86519
		70	251.3272	249.02457
		71	318.08599	249.02457
		71	201.06176	253.16658
		72	184.30661	253.16658
		75	251.3272	261.39842
		79	418.87867	261.39842
		86	234.57205	265.48827
		89	354.41062	269.56073
				269.56073
				273.6158
				285.67672
				301.51455
				328.56143
				339.89217

Initial Power (Exponential Response)

5 Sec. Power	50KHz imp.	linefit
1	64	50.898248
2	34	44.250075
3	43.6	38.400717
3	51	38.400717
3	36.8	38.400717
3	36.4	38.400717
3	16	38.400717
3	47	38.400717
5	9.2	28.815238
5	19.1	28.815238
7	39	21.616219
8	37	18.764635
10	11	14.295998
10	14	14.295998
11	12	12.585068
12	8.1	11.166124
12	9	11.166124
12	18	11.166124
13	7	10.00052
13	7.9	10.00052
13	8	10.00052
13	8	10.00052
13	10	10.00052
13	10	10.00052
14	11.5	9.0527235
14	12.6	9.0527235
15	5	8.2901923
15	8	8.2901923
15	12.1	8.2901923
15	13	8.2901923
17	2	7.2050389
17	4	7.2050389
17	4	7.2050389
17	8.8	7.2050389
17	9.1	7.2050389
19	2	6.540214
20	7.7	6.3125845
22	4.5	5.9817359
23	6.3	5.8509367
23	7.6	5.8509367
26	5.1	5.4725542

27	5.1	5.3268275
30	4.5	4.7719077
30	7	4.7719077
31	5.7	4.5425027
37	3.8	2.7837659
40	0	1.8120993
47	0	0.11371401
48	0	-0.012902438
54	0	-0.12801117
56	0	-0.024695281

Sheath Flow vs. Power

0 Bath flow		2.5 L/min Bath flow		
Sheath flow	5 second power	Sheath	5 sec. power	
0	16	0	36	
0	14	0	27	
0	18	0	35	
0	15	0	30	
5	17	0	39	
5	39	0	26	
5	30	5	40	
5	30	5	53	
10	41	5	43	
10	41	5	38	
10	44	5	34	
10	49	5	30	
10	45	5	38	
15	50	10	64	
15	50	10	66	
15	45	10	71	
15	44	10	60	
20	61	15	72	
20	40	15	67	
20	49	15	86	
20	89	15	69	
20	47	20	70	
25	57	20	79	
25	59	20	75	
25	65	20	63	
25	89	20	57	
25	96	25	69	
25	75	25	65	
30	68	25	67	
30	95	25	58	
30	77	30	71	
30	60	30	89	
		30	66	
		30	60	

sheath	0 flow/5 sec.	std dev.	high	low	linefit
0	15.75	1.4790199	17.22902	14.27098	15.069264
5	29	7.8421936	36.842194	21.157806	31.828463
10	44	2.9664794	46.966479	41.033521	40.068723
15	47.25	2.7726341	50.022634	44.477366	48.305195
20	57.2	17.278889	74.478889	39.921111	59.548485
25	73.5	14.739403	88.239403	58.760597	71.304654
30	75	13.019217	88.019217	61.980783	75.575216

2.5 flow/ 5 sec	std. dev.	high	low	linefit
32.166667	4.8102899	36.976957	27.356377	31.619511
39.428571	6.758215	46.186786	32.670356	41.659065
65.25	3.9607449	69.210745	61.289255	62.30486
73.5	7.4330344	80.933034	66.066966	73.918728
68.8	7.9598995	76.759899	60.840101	71.117048
64.75	4.145781	68.895781	60.604219	62.770743
71.5	10.828204	82.328204	60.671796	72.005282

Bimodal Response

bath	sheath	power	length	width
0	0	8	5.5	5.5
0	0	8	6	6
0	0	8	5.5	5.5
0	0	8	5	5.5
0	0	12	5	5.5
0	0	8	5	5
0	0	17	5.5	5.5
0	0	15	5.5	5.5
0	0	18	5	5
0	0	18	5	5
0	10	38	7.5	7.5
0	10	30	8	8
0	10	30	7.5	7.5
0	10	12	5.5	6
0	20	47	5	5.5
0	20	48	6.5	6.5
0	20	48	6	6.5
0	20	44	4.5	4.5
0	20	46	5	6
0	20	48	7	6.5
0	20	46	7	7.5
0	30	49	6	6
0	30	49	6	6.5
0	30	48	5.5	5.5
1	0	12	5.5	5.5
1	0	11	6	5.5
1	0	10	6.5	5.5
1	10	28	7.5	7.5
1	10	23	8	7.5
1	10	38	7.5	8
1	20	48	7	7.5
1	20	42	6	6.5
1	20	45	6	6.5
1	30	48	7	8
1	30	48	6	7
1	30	47	6.5	7.5
2.5	0	18	6	6.5
2.5	0	15	6.5	6.5
2.5	0	18	7	6

				bath
depth	volume		sheath	0
4.5	142.54965		0	110.64942
3.5	131.94678		10	258.6903
4	126.7108		20	185.31641
3.5	110.87195		30	208.30487
3.5	110.87195		40	156.22865
3	78.53975			
3.5	110.87195			
3.5	110.87195		Bath flow	Sheath flow
3.5	91.629708		0	0
3.5	91.629708			10
3.5	206.16684			20
6	402.12352			30
5	294.52406			40
3.5	131.94678		1	0
3.5	110.87195			10
4	176.97624			20
4.5	199.09827			30
4	84.82293			40
4	150.79632		2.5	0
5	221.2203			10
6	353.42888			20
5.5	207.34494			30
5.5	243.34233			40
5.5	174.22735		5	0
4	126.7108			10
4.5	142.54965			20
4	126.7108			30
5	294.52406			40
5.5	323.97647			
6	402.12352			
5	294.52406			
4.5	199.09827			
4.5	199.09827			
5.5	368.61323			
6	307.87582			
6	353.42888			
5	221.2203			
5.5	243.34233			
5	188.4954			

1	2.5	5	
131.99041	217.68601	288.46996	
340.20802	348.06199	565.70437	
230.90686	227.4053	291.6879	
343.30597	288.15362	253.33433	
257.47948	216.11521	210.09383	
Lesion	Lesion dev.	Lesion high	Lesion low
110.64942	18.665202	129.31462	91.984216
258.6903	100.84615	359.53645	157.84416
185.31641	81.628901	266.94531	103.68751
208.30487	28.224236	236.52911	180.08063
156.22865	0	156.22865	156.22865
131.99041	7.4665053	139.45692	124.52391
340.20802	45.401969	385.60999	294.80605
230.90687	44.984152	275.89102	185.92271
343.30597	25.808435	369.11441	317.49754
257.47948	0	257.47948	257.47948
217.68601	22.530198	240.2162	195.15581
348.06199	30.855117	378.91711	317.20687
227.4053	25.770165	253.17547	201.63514
288.15362	32.087461	320.24108	256.06616
216.11521	0	216.11521	216.11521
288.46996	21.610799	310.08076	266.85916
565.70437	118.79993	684.50429	446.90444
291.6879	27.59433	319.28224	264.09357
253.33433	38.768873	292.1032	214.56545
210.09383	0	210.09383	210.09383

2.5	10	32	7	7
2.5	10	36	7.5	7.5
2.5	10	37	8	7.5
2.5	20	47	6.5	7
2.5	20	48	6	6
2.5	20	48	6.5	6.5
2.5	20	46	7	6.5
2.5	30	47	7	6.5
2.5	30	48	7	7
2.5	30	48	6	6.5
5	0	26	7.5	7.5
5	0	21	7	6.5
5	0	37	7.5	7
5	0	47	6.5	7
5	10	40	8	9.5
5	10	30	9	10
5	10	34	9	8
5	20	48	7	7.5
5	20	48	7	7.5
5	20	40	6.5	7
5	30	48	6.5	7
5	30	49	6	6.5
5	30	49	6.5	7
5	40	48	5	5
5	40	49	7.5	7
5	40	48	6.5	6.5

6	307.87582			
6	353.42888			
6.5	382.88128			
5	256.56318			
5	188.4954			
5	221.2203			
5.5	243.34233			
6	265.46436			
6.5	333.53214			
6	265.46436			
5.5	323.97647			
6	265.46436			
5.5	282.2195			
5.5	282.2195			
6.5	614.31174			
6.5	680.67783			
6	402.12352			
5	294.52406			
5.5	323.97647			
5	256.56318			
4.5	230.90686			
5	221.2203			
6	307.87582			
4	104.71967			
5.5	282.2195			
5.5	243.34233			

Low Voltage Frequency/Impedance Response

Composite data of sheep hearts tested in blood				
This is the composite data taken from: 12-11, 12-11, 1-31, 2-1,				
These tests were performed in sheep blood at approximately 37 c				
	volts 0.5			
30 KHz				
	244	average:	312.25	
	297	stand. dev:	45.762293	
	354			
	354			
50 KHz				
	207	average:	267.5	
	261	atand. dev.:	38.661997	
	297			
	305			
100 KHz				
	203	average:	228	
	239	stand. dev.:	17.986106	
	220			
	250			
200 KHz				
	203	average:	196.75	
	215	stand. dev.:	13.00721	
	183			
	186			
500 KHz				
	189	average:	175.75	
	174	stand. dev.:	7.854139	
	169			
	171			

2-8				
legress				
volts 0.6				volts 0.7
288				208
132	average:	223.2		107
228	stand. dev.:	50.684909		194
228				192
240				214
245				192
126	average	189.4		104
191	stand. dev.	38.066258		168
200				161
185				170
232				168
118	average:	172.6		100
162	stand. dev.:	36.472455		147
173				144
178				145
206				151
114	average:	147.8		93
141	stand. dev.:	30.818176		125
142				131
136				137
180				123
104	average:	128		84
111	stand. dev.:	26.988887		96
125				113
120				100

			volts 0.8	
			177	
average:	183		110	average:
stand. dev.:	38.89473		186	stand. dev:
			193	
			197	
			161	
average:	159		104	average:
stand. dev.:	29.393877		165	stand. dev.:
			168	
			161	
			141	
average:	140.8		100	average:
stand. dev.:	22.22971		140	stand. dev.:
			145	
			137	
			122	
average:	127.4		88	average:
stand. dev.:	19.241622		119	stand. dev.:
			121	
			125	
			105	
average:	103.2		79	average:
stand. dev.:	13.555811		89	stand. dev.:
			97	
			89	

		volts 0.9		
		139		
172.6		118	average:	160
32.028737		180	stand. dev.:	26.88494
		175		
		188		
		131		
151.8		107	average:	141
24.044958		161	stand. dev.:	19.728152
		154		
		152		
		121		
132.6		100	average:	121.6
16.499697		134	stand. dev.:	13.335666
		137		
		116		
		110		
115		93	average:	110.8
13.638182		115	stand. dev.:	9.5582425
		121		
		115		
		97		
91.8		80	average:	88.6
8.7269697		89	stand. dev.:	6.0860496
		93		
		84		

	volts 1.0			
	157			
	98	average:	148	
	172	stand. dev.:	29.35132	
	165			
	143			
	92	average:	133.75	
	155	stand. dev.:	24.529319	
	145			
	128			
	87	average:	119.5	
	133	stand. dev.:	18.848077	
	130			
	114			
	80	average:	105	
	110	stand. dev.:	14.59452	
	116			
	91			
	72	average:	86	
	85	stand. dev.:	8.9721792	
	96			

	0.5	0.6	0.7	0.8
30	312.25	223.2	183	172.6
50	267.5	189.4	159	151.8
100	228	172.6	140.8	132.6
200	196.75	147.8	127.4	115
500	175.75	128	103.2	91.8
	0	0.25	0.5	0.75
30	47.4	102.8	107.4	127
50	46	99.8	103.4	118.4
100	46.8	96.4	98	108.6
200	49	89.6	92	104.4
500	54.2	86.9	87.6	92.2
	max resistance:	180.2		
	0	0.25	0.5	0.75
30	0.26304107	0.57047725	0.59600444	0.70477248
50	0.25527192	0.55382908	0.57380688	0.65704772
100	0.25971143	0.53496115	0.54384018	0.60266371
200	0.27192009	0.49722531	0.51054384	0.57935627
500	0.30077691	0.48224195	0.48612653	0.51165372
0.5	312.25	312.43948	4552.0833	
0.6	223.2	222.25258	-16778.935	
0.7	183	184.89484	22965.521	
0.8	172.6	170.70516	-13949.559	
0.9	160	160.94742	3358.7004	
1	148	147.81052		
0.5	267.5	267.64385	6593.7499	
0.6	189.4	188.68075	-22569.676	
0.7	159	160.43849	28853.021	
0.8	151.8	150.36151	-16413.955	

				This is the
				All tests we
				Data was tak
0.9	1			
160	148			30MHz
141	133.75			
121.6	119.5			
110.8	105			
88.6	86			
1				50 MHz
180.2				
163.6				
145				
123.6				
100.8				
				100 MHz
1				
1				
0.90788013				
0.80466149				
0.68590455				
0.55937847				200 MHz
30000	4552.0833	5630.8477	-2.2931552e-13	
50000	6593.7499	4806.0375	1.9996848e-07	
100000	2437.5	3299.4328	-0.056114344	
200000	2239.5833	2081.844	7140.4979	
500000	406.24999	411.00454		500 MHz
30000	-16778.935	-20143.835	9.7560087e-13	
50000	-22569.676	-16993.414	-8.3206036e-07	
100000	-8726.3888	-11414.944	0.21930544	
200000	-8109.0277	-7617.0046	-26000.485	

composite data of all the sheep hearts done in Krebs solution				
re performed at approximately 37 degrees				
en from the following days: 1-24, 1-23, 2-15				
0.5 Volts				0.6 Volts
282	average:	307.4		276
423	Stand. dev:	71.536284		342
354				282
244				125
234				142
224	average:	268.4		232
392	Stand. dev:	75.064239		254
314				245
183				126
229				121
207	average:	257.6		224
407	Stand. dev:	85.143643		245
297				196
177				116
200				102
183	average:	231		180
379	Stand. dev:	81.301906		240
255				175
152				93
186				101
159	average:	205.8		160
366	Stand. dev:	85.611681		173
220				132
127				84
157				92

			0.7 Volts	
average:	233.4		227	average:
Stand. dev:	84.941392		288	Stand. dev:
			230	
			94	
			94	
average:	195.6		211	average:
Stand. dev:	59.304637		223	Stand. dev:
			214	
			83	
			93	
average:	176.6		187	average:
Stand. dev:	57.513824		197	Stand. dev:
			178	
			72	
			80	
average:	157.8		164	average:
Stand. dev:	54.718918		176	Stand. dev:
			147	
			66	
			74	
average:	128.2		130	average:
Stand. dev:	35.487463		148	Stand. dev:
			113	
			61	
			66	

		0.8 Volts		
186.6		226	average:	175.4
78.672994		236	Stand. dev:	66.28303
		226		
		101		
		88		
164.8		204	average:	159.2
62.91073		226	Stand. dev:	62.923446
		200		
		88		
		78		
142.8		180	average:	133.6
54.930502		180	Stand. dev:	50.297515
		163		
		75		
		70		
125.4		163	average:	117.8
46.232456		157	Stand. dev:	45.578065
		144		
		64		
		61		
103.6		125	average:	93
34.598266		118	Stand. dev:	28.892906
		105		
		58		
		59		

	0.9 Volts			
	206	average:	156.4	
	211	Stand. dev:	55.916366	
	186			
	103			
	76			
	188	average:	142.4	
	195	Stand. dev:	50.874748	
	165			
	70			
	94			
	157	average:	119	
	154	Stand. dev:	39.217343	
	140			
	81			
	63			
	136	average:	105.6	
	145	Stand. dev:	35.409603	
	120			
	68			
	59			
	107	average:	84.2	
	106	Stand. dev:	23.025204	
	95			
	58			
	55			

1.0 Volts				30
205	average:	158.6		50
207	Stand. dev:	56.10205		100
201				200
86				500
94				
189	average:	134.4		30
170	Stand. dev:	45.565777		50
152				100
83				200
78				500
164	average:	121.2		
155	Stand. dev:	42.154003		
147				30
69				50
71				100
				200
				500
139	average:	104		
132	Stand. dev:	34.583233		
125				
61				
63				
113	average:	84.8		
101	Stand. dev:	23.701477		
97				
56				
57				

0.5	0.6	0.7	0.8	0.9
307.4	233.4	186.6	175.4	156.4
268.4	195.6	164.8	159.2	142.4
257.6	176.6	142.8	133.6	119
231	157.8	125.4	117.8	105.6
205.8	128.2	103.6	93	84.2
0	0.25	0.5	0.75	1
78.666667	136.66667	137.66667	164.66667	239.33333
79.666667	132.33333	131.66667	155.33333	215.66667
78.666667	127.66667	132.33333	147	185
80	122.66667	126	133.33333	156.33333
80.333333	116	119.33333	124.66667	128
max resistan	239.33333			
0	0.25	0.5	0.75	1
0.32869081	0.57103064	0.57520891	0.68802228	1
0.33286908	0.55292479	0.55013928	0.64902507	0.90111421
0.32869081	0.53342618	0.55292479	0.61420613	0.7729805
0.33426184	0.51253482	0.5264624	0.55710306	0.65320334
0.3356546	0.48467967	0.49860724	0.52089136	0.53481894

			Comparison dat
			0
1		30	0.065649742
158.6		50	0.077597161
134.4		100	0.068979376
121.2		200	0.06234175
104		500	0.034877682
84.8			

a - difference in normalized graphs			
0.25	0.5	0.75	1
0.00055339317	-0.020795526	-0.016750191	0
-0.00090428771	-0.023667605	-0.0080226551	-0.0067659271
-0.0015349704	0.0090846135	0.011542421	-0.031680986
0.015309514	0.015918555	-0.022253207	-0.032701208
0.0024377124	0.012480716	0.0092376468	-0.024559527

	Normalized Krebs Data for each test			
	282	276	227	226
	224	232	211	204
	207	224	187	180
	183	180	164	163
	159	160	130	125
	1	0.9787234	0.80496454	0.80141844
	1	1.0357143	0.94196429	0.91071429
	1	1.0821256	0.90338164	0.86956522
	1	0.98360656	0.89617486	0.89071038
	1	1.0062893	0.81761006	0.78616352
	0.5	0.6	0.7	0.8
mean	1	1.0172918	0.87281908	0.85171437
	0.5	0.6	0.7	0.8
high	1	1.0821256	0.94196429	0.91071429
low	1	0.9787234	0.80496454	0.78616352
new high	1	1.0554653	0.92556924	0.90100316
new low	1	0.97911833	0.82006892	0.80242558
Stand. Dev	0	0.038173503	0.052750159	0.049288794

				Mean for the
				0.5
206	205			
188	189			282
157	164			229
136	139			207
107	113			186
				159
				Standard dev.
0.73049645	0.72695035			71.536284
0.83928571	0.84375			75.064239
0.75845411	0.79227053			85.143643
0.7431694	0.75956284			81.301906
0.67295597	0.71069182			85.611681
0.9	1			
			high	353.53628
0.74887233	0.76664511		low	210.46372
0.9	1			
0.83928571	0.84375		high	304.06424
0.67295597	0.71069182		low	153.93576
0.80253774	0.81430731			
0.69520692	0.71898291		high	292.14364
0.053665407	0.047662204		low	121.85636
			high	267.30191
			low	104.69809
			high	244.61168
			low	73.388319

Krebs data				
0.6	0.7	0.8	0.9	1
276	227	226	186	201
232	211	200	165	152
196	178	163	140	147
175	147	144	120	125
132	113	105	95	97
s.				
84.941392	78.672994	66.28303	55.916366	56.10205
59.304637	62.91073	62.923446	50.874748	45.565777
57.513824	54.930502	50.297515	39.217343	42.154003
54.718918	46.232456	45.578065	35.409603	34.583233
35.487463	34.598266	28.892906	23.025204	23.701477
360.94139	305.67299	292.28303	241.91637	257.10205
191.05861	148.32701	159.71697	130.08363	144.89795
291.30464	273.91073	262.92345	215.87475	197.56578
172.69536	148.08927	137.07655	114.12525	106.43422
253.51382	232.9305	213.29751	179.21734	189.154
138.48618	123.0695	112.70249	100.78266	104.846
229.71892	193.23246	189.57806	155.4096	159.58323
120.28108	100.76754	98.421935	84.590397	90.416767
167.48746	147.59827	133.89291	118.0252	120.70148
96.512537	78.401734	76.107094	71.974796	73.298523

	"Normalized data in Krebs"			
	0.5	0.6	0.7	0.8
	1	0.9787234	0.80496454	0.80141844
	0.81205674	0.82269504	0.74822695	0.70921986
	0.73404255	0.69503546	0.63120567	0.57801418
	0.65957447	0.62056738	0.5212766	0.5106383
	0.56382979	0.46808511	0.40070922	0.37234043
	0.25367477	0.30121061	0.27898225	0.2350462
	0.26618525	0.21030013	0.2230877	0.22313279
	0.30192781	0.20394973	0.19478901	0.17835998
	0.28830463	0.19403872	0.16394488	0.16162434
	0.30358752	0.12584207	0.12268889	0.10245711

			"Normalized to self"	
0.9	1		0.5	0.6
0.65957447	0.71276596		1	0.9787234
0.58510638	0.53900709		1	1.0131004
0.4964539	0.5212766		1	0.9468599
0.42553191	0.44326241		1	0.94086022
0.33687943	0.34397163		1	0.83018868
			"Standard devs. using all	
0.19828499	0.19894344		0.25367477	0.30121061
0.18040691	0.16158077		0.32779144	0.25897222
0.13906859	0.14948228		0.41132195	0.27784456
0.12556597	0.12263558		0.43710702	0.29418773
0.081649658	0.08404779		0.53843825	0.22319159
			"Standard devs. removing	
			0.073324172	0.10567138
			0.08998883	0.039435858
			0.061907835	0.096966629
			0.082631841	0.15878177
			0.092052404	0.10759436
		high	1.0733242	1.0843948
		low	0.92667583	0.87305203
		high	1.0899888	1.0525363
		low	0.91001117	0.97366458
		high	1.0619078	1.0438265
		low	0.93809216	0.84989327
		high	1.0826318	1.099642
		low	0.91736816	0.78207845
		high	1.0920524	0.93778304
		low	0.9079476	0.72259432

0.7	0.8	0.9	1	
0.80496454	0.80141844	0.65957447	0.71276596	
0.92139738	0.87336245	0.72052402	0.66375546	
0.85990338	0.78743961	0.6763285	0.71014493	
0.79032258	0.77419355	0.64516129	0.67204301	
0.71069182	0.66037736	0.59748428	0.61006289	
the data				
0.27898225	0.2350462	0.2350462	0.2350462	
0.27471935	0.27477487	0.27477487	0.27477487	
0.26536474	0.24298316	0.24298316	0.24298316	
0.24856159	0.24504336	0.24504336	0.24504336	
0.21759916	0.18171639	0.18171639	0.18171639	
outliers				
0.099557786	0.016716472	0.016716472	0.016716472	
0.022266461	0.049916822	0.049916822	0.049916822	
0.037489361	0.038714381	0.038714381	0.038714381	
0.063966195	0.042635761	0.042635761	0.042635761	
0.089878202	0.052116574	0.052116574	0.052116574	
0.90452232	0.81813491	0.67629094	0.72948243	
0.70540675	0.78470197	0.642858	0.69604949	
0.94366384	0.92327927	0.77044084	0.71367228	
0.89913092	0.82344562	0.6706072	0.61383864	
0.89739274	0.82615399	0.71504288	0.74885931	
0.82241402	0.74872523	0.63761412	0.67143055	
0.85428878	0.81682931	0.68779705	0.71467877	
0.72635639	0.73155779	0.60252553	0.62940725	
0.80057003	0.71249393	0.64960085	0.66217947	
0.62081362	0.60826078	0.5453677	0.55794632	

	0.5 Volts			0.6 Volts
	282	1		276
	423	1.5		342
	354	1.2553191		282
	244	0.86524823		125
	234	0.82978723		142
	224	0.97816594		232
	392	1.7117904		254
	314	1.371179		245
	183	0.79912664		126
	229	1		121
	207	1		224
	407	1.9661836		245
	297	1.4347826		196
	177	0.85507246		116
	200	0.96618357		102
	183	0.98387097		180
	379	2.0376344		240
	255	1.3709677		175
	152	0.8172043		93
	186	1		101
	159	1		160
	366	2.3018868		173
	220	1.3836478		132
	127	0.79874214		84
	157	0.98742138		92

		0.7 Volts		
0.9787234		227	0.80496454	
1.212766		288	1.0212766	
1		230	0.81560284	
0.44326241		94	0.33333333	
0.5035461		94	0.33333333	
1.0131004		211	0.92139738	
1.1091703		223	0.97379913	
1.069869		214	0.93449782	
0.55021834		83	0.36244541	
0.52838428		93	0.40611354	
1.0821256		187	0.90338164	
1.1835749		197	0.95169082	
0.9468599		178	0.85990338	
0.56038647		72	0.34782609	
0.49275362		80	0.38647343	
0.96774194		164	0.88172043	
1.2903226		176	0.94623656	
0.94086022		147	0.79032258	
0.5		66	0.35483871	
0.54301075		74	0.39784946	
1.0062893		130	0.81761006	
1.0880503		148	0.93081761	
0.83018868		113	0.71069182	
0.52830189		61	0.3836478	
0.57861635		66	0.41509434	

0.8 Volts			0.9 Volts	
226	0.80141844		206	0.80141844
236	0.83687943		211	0.83687943
226	0.80141844		186	0.80141844
101	0.35815603		103	0.35815603
88	0.31205674		76	0.31205674
204	0.89082969		188	0.89082969
226	0.98689956		195	0.98689956
200	0.87336245		165	0.87336245
88	0.38427948		70	0.38427948
78	0.34061135		94	0.34061135
180	0.86956522		157	0.86956522
180	0.86956522		154	0.86956522
163	0.78743961		140	0.78743961
75	0.36231884		81	0.36231884
70	0.33816425		63	0.33816425
163	0.87634409		136	0.87634409
157	0.84408602		145	0.84408602
144	0.77419355		120	0.77419355
64	0.34408602		68	0.34408602
61	0.32795699		59	0.32795699
125	0.78616352		107	0.78616352
118	0.74213836		106	0.74213836
105	0.66037736		95	0.66037736
58	0.36477987		58	0.36477987
59	0.37106918		55	0.37106918

	1.0 Volts	
	205	0.80141844
	207	0.83687943
	201	0.80141844
	86	0.35815603
	94	0.31205674
	189	0.89082969
	170	0.98689956
	152	0.87336245
	83	0.38427948
	78	0.34061135
	164	0.86956522
	155	0.86956522
	147	0.78743961
	69	0.36231884
	71	0.33816425
	139	0.87634409
	132	0.84408602
	125	0.77419355
	61	0.34408602
	63	0.32795699
	113	0.78616352
	101	0.74213836
	97	0.66037736
	56	0.36477987
	57	0.37106918

	0 depth			
30 KHz	51			
	55	average:	47.4	
	49	stand. dev.:	6.406247	
	46			
	36			
50 KHz	53			
	53	average:	46	
	47	stand. dev.:	6.8702256	
	42			
	35			
100 KHz	53			
	54	average:	46.8	
	48	stand. dev.:	6.910861	
	44			
	35			
200 KHz	55			
	56	average:	49	
	50	stand. dev.:	6.8410526	
	47			
	37			
500 KHz	60			
	60	average:	54.2	
	58	stand. dev.:	6.9397406	
	51			
	42			

0.25 depth				0.5 depth
127				126
100	average:	102.8		115
125	stand. dev.:	20.536796		102
87				100
75				94
128				120
100	average:	99.8		111
121	stand. dev.:	22.96432		102
84				92
66				92
122				117
95	average:	96.4		107
115	stand. dev.:	20.401961		97
84				87
66				82
117				110
88	average:	89.6		100
105	stand. dev.:	19.438107		92
74				83
64				75
120				111
87	average:	86.9		96
94	stand. dev.:	19.970979		88
71				75
62.5				68

			0.75 depth	
			140	
average:	107.4		122	average:
stand. dev.:	11.551623		148	stand. dev.:
			117	
			108	
			137	
average:	103.4		117	average:
stand. dev.:	10.910545		138	stand. dev.:
			106	
			94	
			128	
average:	98		109	average:
stand. dev.:	12.806248		122	stand. dev.:
			97	
			87	
			125	
average:	92		106	average:
stand. dev.:	12.312595		120	stand. dev.:
			90	
			81	
			113	
average:	87.6		96	average:
stand. dev.:	15.239423		106	stand. dev.:
			77	
			69	

		1 depth		
		241		
127		170	average:	180.2
14.805404		189	stand. dev.:	35.571899
		132		
		169		
		217		
118.4		164	average:	163.6
17.211624		174	stand. dev.:	32.512152
		120		
		143		
		197		
108.6		150	average:	145
15.213152		150	stand. dev.:	30.996774
		106		
		122		
		164		
104.4		123	average:	123.6
16.883128		127	stand. dev.:	22.738514
		100		
		104		
		132		
92.2		109	average:	100.8
16.773789		104	stand. dev.:	19.813127
		81		
		78		

0.9	141	141.71925	3670.4663	
1	133.75	133.60615		
0.5	228	228.25595	2437.5	
0.6	172.6	171.32024	-8726.3888	
0.7	140.8	143.35952	11866.875	
0.8	132.6	130.04048	-7317.4682	
0.9	121.6	122.87976	1858.7262	
1	119.5	119.24405		
0.5	196.75	196.62798	2239.5833	
0.6	147.8	148.41012	-8109.0277	
0.7	127.4	126.17976	11035.729	
0.8	115	116.22024	-6745.0258	
0.9	110.8	110.18988	1683.8631	
1	105	105.12202		
0.5	175.75	175.72321	406.24999	
0.6	128	128.13393	-2397.9166	
0.7	103.2	102.93214	4554.0625	
0.8	91.8	92.067857	-3575.8512	
0.9	88.6	88.466072	1099.4821	
1	86	86.026786		

500000	-2397.9166	-2412.7471		
				30MHz
30000	22965.521	26815.043	-1.4301873e-12	
50000	28853.021	22473.649	1.2067131e-06	
100000	11866.875	14942.643	-0.30659881	
200000	11035.729	10472.843	34965.58	
500000	4554.0625	4571.0289		
				50MHz
30000	-13949.559	-15850.407	8.826748e-13	
50000	-16413.955	-13263.897	-7.4134525e-07	
100000	-7317.4682	-8836.246	0.184308	
200000	-6745.0258	-6467.0795	-20736.269	
500000	-3575.8512	-3584.229		
				100 MHz
30000	3358.7004	3694.6447	-2.0190558e-13	
50000	3670.4663	3113.7444	1.6938644e-07	
100000	1858.7262	2127.1457	-0.041606592	
200000	1683.8631	1634.7406	4795.8461	
500000	1099.4821	1100.9628		
				200 MHz
				500 MHz

0				0.25
82	average:	78.666667		137
86	Stand. dev:	7.7172246		153
68				120
85	average:	79.666667		135
84	Stand. dev:	6.8475462		150
70				112
81	average:	78.666667		129
87	Stand. dev:	7.9302515		147
68				107
82	average:	80		129
89	Stand. dev:	8.2865353		136
69				103
82	average:	80.333333		132
86	Stand. dev:	5.4365021		122
73				94

			0.5	
average:	136.66667		151	average:
Stand. dev:	13.474255		148	Stand. dev:
			114	
average:	132.33333		138	average:
Stand. dev:	15.627611		144	Stand. dev:
			113	
average:	127.66667		151	average:
Stand. dev:	16.357126		142	Stand. dev:
			104	
average:	122.66667		136	average:
Stand. dev:	14.197026		142	Stand. dev:
			100	
average:	116		137	average:
Stand. dev:	16.083117		126	Stand. dev:
			95	

		0.75		
137.66667		161	average:	164.66667
16.779617		180	Stand. dev:	11.323525
		153		
131.66667		156	average:	155.33333
13.424687		170	Stand. dev:	12.256518
		140		
132.33333		154	average:	147
20.368821		159	Stand. dev:	13.589211
		128		
126		151	average:	133.33333
18.547237		136	Stand. dev:	15.627611
		113		
119.33333		144	average:	124.66667
17.782638		126	Stand. dev:	16.357126
		104		

	1			
	241	average:	239.33333	
	250	Stand. dev:	9.4633797	
	227			
	220	average:	215.66667	
	227	Stand. dev:	11.440668	
	200			
	200	average:	185	
	189	Stand. dev:	14.165686	
	166			
	170	average:	156.33333	
	159	Stand. dev:	12.391754	
	140			
	140	average:	128	
	136	Stand. dev:	14.236104	
	108			

				Data for NAS
				Impedance vs
				1
			30	180.2
			50	163.6
			100	145
			200	123.6
			500	100.8
				Normal Imped
	correl(depth	correl(freq,ohm)		1
	0.95801826	-0.91922167	30	1
	0.95139413	-0.90934414	50	0.90788013
	0.93846434	-0.89376215	100	0.80466149
	0.94580078	-0.88906205	200	0.68590455
	0.87809613	0.97567999	500	0.55937847
				Impedance vs
	correl(freq,	correl(freq, ohms)		
	-0.89786202	-0.82661931		30
	-0.88116883	-0.86321744		50
	-0.90272287	-0.89554253		100
	-0.90497272	-0.90502165		200
	-0.8902794	-0.89762157		500
		-0.91995289		
				Normalized I
				30
				50
				100
				200
				500

PE graphs				
. depth vs. freq.				
0.75	0.5	0.25	0	
127	107.4	102.8	47.4	
118.4	103.4	99.8	46	
108.6	98	96.4	46.8	
104.4	92	89.6	49	
92.2	87.6	86.9	54.2	
ance vs. depth. vs. Freq.				
0.75	0.5	0.25	0	
0.70477248	0.59600444	0.57047725	0.26304107	
0.65704772	0.57380688	0.55382908	0.25527192	
0.60266371	0.54384018	0.53496115	0.25971143	
0.57935627	0.51054384	0.49722531	0.27192009	
0.51165372	0.48612653	0.48224195	0.30077691	
. Freq.				
0.5	0.6	0.7	0.8	0.9
312.25	223.2	183	172.6	160
267.5	189.4	159	151.8	141
228	172.6	140.8	132.6	121.6
196.75	147.8	127.4	115	110.8
175.75	128	103.2	91.8	88.6
mpedance vs. Freq.				
0.5	0.6	0.7	0.8	0.9
1	0.71481185	0.58606886	0.55276221	0.51240993
0.85668535	0.60656525	0.50920737	0.48614892	0.45156125
0.73018415	0.55276221	0.45092074	0.42465973	0.38943155
0.63010408	0.47333867	0.40800641	0.36829464	0.35484388
0.56285028	0.40992794	0.3305044	0.2939952	0.283747

Standard Deviations			
	1	0.75	0.5
30	35.571899	14.805404	11.551623
50	32.512152	17.211624	10.910545
100	30.996774	15.213152	12.806248
200	22.738514	16.883128	12.312595
500	19.813127	16.773789	15.239423
	1	0.75	0.5
30	0.19740233	0.082160957	0.064104458
50	0.18042259	0.095514007	0.060546867
100	0.17201317	0.084423708	0.071066862
200	0.12618487	0.093691053	0.068327387
500	0.10995076	0.09308429	0.084569493
1			
148			
133.75			
119.5			
105			
86			
1			
0.47397918			
0.42834267			
0.38270616			
0.33626902			
0.27542034			

			Low Data
0.25	0		
20.536796	6.406247		30
22.96432	6.8702256		50
20.401961	6.910861		100
19.438107	6.8410526		200
19.970979	6.9397406		500
0.25	0		
0.11396668	0.03555076		
0.12743796	0.038125558		
0.11321843	0.03835106		
0.10786963	0.037963666		
0.11082674	0.038511324		

1	0.75	0.5	0.25	0
144.6281	112.1946	95.848377	82.263204	40.993753
131.08785	101.18838	92.489455	76.83568	39.129774
114.00323	93.386848	85.193752	75.998039	39.889139
100.86149	87.516872	79.687405	70.161893	42.158947
80.986873	75.426211	72.360577	66.929021	47.260259

	High Data			
		1	0.75	0.5
	30	215.7719	141.8054	118.95162
	50	196.11215	135.61162	114.31055
	100	175.99677	123.81315	110.80625
	200	146.33851	121.28313	104.3126
	500	120.61313	108.97379	102.83942

0.25	0			
123.3368	53.806247			
122.76432	52.870226			
116.80196	53.710861			
109.03811	55.841053			
106.87098	61.139741			

Bibliography

[1] Vedel J, Frank, Fontaine G, et al. Bloc auriculo-ventriculaire intra-Hisen definitif induit au cours d'une exploration endoventriculaire droite, *Arch Mal Coeur Vaiss,* 72:107-112, 1979

[2] E.G.C.A. Boyd and P.M. Holt, The Biophysics of catheter ablation techniques, *Journal of Electrophysiology,* Vol.1, No. 1, 62-75, 1987

[3] Saul, J. Philip, Electrophysiologic Therapeutic Catheterization

[4] Wonnell TL, Stauffer PR, Langberg JJ, Evaluation of microwave and radiofrequency cather ablation in a myocardium-equivalent phantom model, IEEE Trans. Biomed. Eng, 39:1086 - 1095, 1992

[5] Langberg JJ, Wonnell TL, Chin MC, et. al., Cathether ablation of the atrioventricular junction using a heclical microwave antenna: a novel means of coupling energy to the endocardium, *J Electrophysiol* (in press)

[6] Haines DE, Whayne JG, What is the radial temperature profile achieved during microwave catheter ablation with a helical coil antenna in cainine myocardium? [Abstract] *J Am Coll Cardiol,* 19:99a, 1992

[7] Gillette P, Armenia J., Swindle M, et al., Transvenous cryoablation of atrioventricular conduction [Abstract] *PACE Pacing Clin Electrophysiol,* 12:676, 1989

[8] Haines DE, Thermal ablation of perfused porcine left ventricle in vitro with the neodymium-YAG laser hot tip catheter system, *PACE Pacing Clin Electrophysiol,* 15:979-985, 1992

[9] Downar E, Butany J, Jares A, Stoicheff BP, Endocardial photoablation by excimer laser, *J Am Coll Cardiol,* 7:546-550, 1986

[10] Svenson RH, Littmann L, Colavita P, et al., Laser photoablation of ventricular tachycardia: correlation of diastolic activation times and photoablation effects on cycle length and termination - observations supporting a macroreentrant mechanism, *J Am Coll Cardiol,* 19:607 - 613, 1992

[11] Nath Sunil, DiMarco John P., Haines David, Basic Aspects of Radiofrequency Catheter Ablation, *Journal of Cardiovascular Electrophysiology,* Vol. 5., 10:863-876, 1994

[12] Haines David E., The biophysics of radiofrequency catherer ablation in the heart: the

importance of temperature monitoring, PACE, Vol.16:586 - 591, 1993

[13] Cosman Eric R., Rittman William J., Nashold Blaine S., Makachinas Thad T., Radiofrequency lesion generation and its effects on tissue impedance, *Appl. Neurophysiol.*, 51: 230-242 (1988)

[14] Haines David E., Verow Anthony F., Observations on electrode-tissue interface temperatur and effect on electrical impedance during radiofrequency ablation of ventricular myocardium, Circulation, Vol. 82, 3:1034-1038 (1990)

[15] Guyton Arthur G., The Textbook of Medical Physiology 8th Ed., Philadelphia, W.B. Saunders Co., 1991

[16] Katz Arnold M., Physiology of the Heart 2nd Ed., New york, Raven Press, 1992

[17] Mark Roger, Kamm Roger D., Quantitative Physiology: Organ Transport Systems, Class Notes, Spring 1997

[18] De Wang, Hulse J. Edward, Erickson Christopher, Walsh Edward, Saul, J. Philip, Factors influencing impedance during radiofrequency ablation in humans

[19] Berne Robert M., Levy Mathew N., Cardiovascular Physiology 6th Ed., St. Louis, Mosby-Year Book, 1992

[20] Grodzinski Alan, Fields, Forces and Flows: Backgroud for Physiology, Course Notes, Fall semester 1995